Ecological Indicators 178 (2025) 114087

Contents lists available at ScienceDirect

Ecological Indicators

journal homepage: www.elsevier.com/locate/ecolind

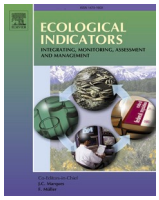

Original Articles

Assessing relative contributions of climate and socio-environmental factors to ecosystem health through space–time interpretable machine learning

Xiaoliang Meng [a], Junyi Wu [a], Yichun Xie [b,*], Yongfei Bai [c], Chenghu Zhou [d], Yuchen Li [e,f]

[a] School of Remote Sensing and Information Engineering, Wuhan University, Wuhan 430079, China
[b] Department of Geography and Geology, Eastern Michigan University, USA
[c] Institute of Botany, Chinese Academy of Sciences, Beijing, China
[d] Institute of Geographic Sciences and Natural Resources Research, Chinese Academy of Sciences, Beijing, China
[e] MRC Epidemiology Unit, School of Clinical Medicine, University of Cambridge, Cambridge CB2 0QQ, UK
[f] Institute for Spatial Data Science, School of Geography, University of Leeds, Leeds LS2 9JT, UK

ARTICLE INFO

Keywords:
Relative contributions of coupled climate and socioenvironmental factors
Interpretable machine learning
Fine-grained spatial and temporal analysis
Each feature's contribution to individual prediction (EFCTIP)
Localized EFCTIP

ABSTRACT

The biggest challenge of sustainability is improving ecosystem production services while preserving other functions at large scales. One solution is to seek a delicate equilibrium from complex nonlinear trade-offs between socioeconomic development, climate change, and environmental protection to maximize ecosystem services. This solution's thrust is understanding these factors' relative contributions (RC) to long-term ecosystem changes. Here, we developed a novel analysis based on space–time interpretable machine learning (IML) to assess the RC from two climate factors, four land uses, four environmental pollution indicators, and 28 socioeconomic variables from 2001 to 2018 on grassland changes across the Inner Mongolia Plateau. Compared with econometric panel regression analysis and hierarchical linear mixed models, which are popular in ecological and geographical studies, the IML models generated exciting insights and illustrated several advantages. The IML models identified that no driving factors have maintained consistent impacts on ecosystem health in space and time. The strengths and directions of their RC varied and depended on their regional and local interactions. The IML models revealed fine-grained space–time RC variations, with each feature contributing to individual predictions (EFCTIP), and EFCTIP varying regionally and locally, which no other approaches can achieve. Traditional models' system-wide interpretations are misleading. The IML models support the concurrent spatiotemporal examination of ecosystem health and feature engineering to mitigate limitations from multicollinearity and non-linearity. This study has significant policy implications for grassland management in Inner Mongolia and can be applied to other ecosystems.

1. Introduction

Over the past decade, the focus of ecosystem health research has shifted increasingly from quantitative evaluation to the analysis of driving forces and mechanisms (He et al., 2024). This shift signifies several important new efforts. One emphasis is on a total socio-environmental system approach (Xie, 2023) or a tightly coupled human nature system method (Hull et al., 2015; Gupta, 2020; Shi, 2021) to synthesize how human factors (economic growth, demographic shift, environmental pollution, land use changes, regional development policies, urbanization, etc.) and natural environments (climate changes, geologic factors, hydrological dynamics, natural resource consumption, etc.) interactively affect ecosystem health. The concept of a total or integrated socioenvironmental system can be traced back to the theory of coevolution between nature and society (Norgaard and Kallis, 2011). When a living society consumes resources from a biophysical system for socioeconomic well-being, the residents alter the biophysical system and also adjust to the changes their consumption caused (Weisz and Clark, 2011). This concept has inspired new interests in exploring nature-society coevolution in recent years because the tradeoff between human alteration and adaptation impacts socioenvironmental sustainability (Waring et al., 2017; Fischer et al., 2021; Zhou et al., 2022).

A related effort to support the study of total or integrated socio-environmental systems involves compiling and creating comprehensive data that encompasses both environmental and socioeconomic factors from an increasingly growing number of sources (Zhou et al., 2022). Big

* Corresponding author.
E-mail address: yxie@emich.edu (Y. Xie).

https://doi.org/10.1016/j.ecolind.2025.114087
Received 27 May 2025; Received in revised form 3 August 2025; Accepted 18 August 2025
Available online 24 August 2025

data makes high-resolution spatial and temporal data available to ecologists and geoscientists over large areas. These fine-grained ecological data, including ground-based images, can be used to develop innovative approaches for habitat mapping, leveraging multimodal data and computer vision (Morueta-Holme et al., 2023). They can be used to develop functional indicators to measure ecosystem health (Hu et al., 2022). Big data complements ecological experiments to advance ecology and conservation (McCleery, 2023). For example, in a study of the Inner Mongolia Autonomous Region (IMAR) grassland spatial distribution patterns, remote sensing data from the online Google Earth Engine platform, along with 6114 field plots, over 23 years (2000–2022) were analyzed and mapped (Yang, 2024).

On the other hand, more environmental scientists are paying attention to socioeconomic factors that are crucial for measuring human well-being, a critical societal element of sustainability (O'Neill et al., 2018). Based on the public well-being measurement summarized by Forgeard et al. (2011), the following socioeconomic variables (Forgeard et al., 2011), such as, gross domestic productivity (GDP), income, economic activities, education, democratic quality, governmental investment, employment, and markets, are often analyzed along with environmental indicators in the literature concerning ecosystem health. For example, time series data on grassland productivity and climatic changes (nine growing seasons ×18 years from 2000 to 2017) with yearly observations of ten socioeconomic variables were assembled to investigate how these factors affected grassland deterioration in IMAR (Zhou et al., 2022).

Another accompanying effort is to develop more advanced and integrated modeling frameworks to analyze total or integrated socio-environmental systems with increasing volumes of large and combined socioenvironmental datasets. Current research methods concerning the relative contributions of socioenvironmental factors can be summarized into four groups. The first group comprises process-based models that integrate climate, hydrological, water quality, and ecological models to examine aquatic environments (Shrestha, 2024). Popular models include general circulation models (Li et al., 2023), regional circulation models (Li et al., 2023); modified vegetation photosynthesis model (Gong et al., 2024); the Soil and Water Assessment Tool (Shrestha, 2024), the Planification et gestion de l'assainissement des eaux (PEGASE) model (Boukari, 2019), and dynamic land use change models (Shiferaw et al., 2025). These models are primarily focused on hydrological and environmental processes and their impacts on ecosystem health, but are less detailed on anthropogenic factors (Koppa et al., 2022).

The second group pertains to comprehensive index assessment models, which have been emerging and applied in many ecological studies. Vigor-organization-resilience model, pressure-state-response model, and vigor-organization-resilience-ecosystem services (VORS) model are some typical examples (Shen, 2023). For example, A VORS was adopted to assess the ecosystem health of the Southern China Karst landscape from 2004 to 2020 (He et al., 2024). These models primarily originate from disciplines such as agriculture, ecology, resource conservation, land use management, environmental monitoring, geographical information science, and sustainable development. The socioeconomic factors are narrowly defined and usually include socio-economic measures of ecological engineering intervention, such as environmental protection investment, area of artificial wetlands, and length of new pipelines (Yuan, 2023) in addition to several standard socioeconomic variables, including GDP (Gross domestic product), population density, urbanization, and agricultural production. However, much information concerning industrial structure (such as the proportion of secondary and tertiary industries), pollution states, residents' well-being (income and access to health), and social development (transportation and education facilities) is seldom accounted for.

Empirical statistical models belong to the third group, which analyzes linear relationships between a response variable and a set of explanatory variables to examine how these drivers affect the response (Schulz, 2020). Typical statistical models include multiple regression models, structural equation models (SEM), econometric panel regression analysis (EPRA), and hierarchical linear mixed model (HLMM). These models usually examine balanced sets of variables covering biophysical and socioeconomic factors (Zhou et al., 2022). EPRA and HLMM are more capable of handling complex data structures than regression and SEM models. EPRA is a popular and influential method to simultaneously analyze the impacts of climate and socioeconomic factors on an ecosystem's cross-area (spatial) and time-series (temporal) variations (Xie et al., 2021). EPRA can examine multilevel regional differences over time and allow more sample variability (Hsiao, 2007). EPRA provides a greater capacity for capturing the complexity of human behavior than a single time-series or cross-section data (Hsiao, 2022).

HLMM is a multilevel mixed model to describe causal relationships between an ecological issue and its potential driving factors (Hedeker and Gibbons, 2006; Price et al., 2016). HLMM incorporates random effects to examine heterogeneities among individuals, species, communities, regions, and periods (Bolker, 2015). Therefore, HLMM can currently handle random effects and repeated measures to support the analysis of hierarchical (multilevel) relationships (Bolker, 2010). Modeling the grouping variable using so-called random effects in a mixed effects model is a significant improvement compared to modeling each group separately or including a grouping variable as a categorical variable in a model (Sigrist, 2022). However, treating a grouping variable as random effects in HLMM is less flexible than treating a formal cross-section and over-time (spatiotemporal) structure in EPRA.

In recent years, machine learning (ML) techniques have been increasingly expanding and providing innovative solutions to overcome the limitations of conventional statistical models (Reichstein, 2019). Many ML approaches have been applied in ecology and evolution (Stock et al., 2023), environment science (Wegmann and Jaume-Santero, 2023), earth science (Bergen et al., 2019), and geoscience (Chen, 2024). A machine learning-based hybrid model has been developed to estimate global terrestrial evaporation (Koppa et al., 2022). The constraints affecting evaporation from plant leaves (or transpiration) are particularly complex. They are often assumed to interact linearly in global models due to our limited knowledge based on local studies. Machine learning has broken these limitations and improved the estimation of evaporation. Schulz and his team (Schulz, 2020) have done an interesting experiment, systematically assessing the performance of linear, shallow-nonlinear, and machine learning models as a function of sample size on UKBiobank brain images against established machine learning references. They confirmed that prediction accuracy constantly improves from the linear models to the shallow-nonlinear and machine-learning nonlinear models.

Animal ecologists can utilize large datasets from modern sensors. Integrating machine learning approaches with domain knowledge improves inputs for ecological models and leads to integrated hybrid modeling tools for better wildlife preservation (Tuia, 2022). Andermann et al. (2022) have demonstrated how machine learning can harness unexplored signals from complex data sets that traditional methods cannot (Andermann et al., 2022). Thus, integrating machine learning can extract information from fossil evidence, geologic models, and paleoclimatic proxies to reconstruct paleo vegetation and provide insights into the evolution of Earth's biomes in time and space. Wu and her colleagues (2022) have demonstrated the use of machine learning to automatically count huge populations of mammals across a highly heterogeneous landscape (Wu, 2023). They developed a robust machine-learning tool that automatically locates and counts large herds of migratory wildebeest and zebra in the Serengeti-Mara ecosystem. Brun et al. (2024) applied deep neural networks (DNNs) to ubiquitous citizen science data to identify the distributions of 2477 plant species and species aggregates across Switzerland (Brun, 2024). They found that compared to commonly used approaches, multispecies DNNs predict species distributions and especially community composition more accurately. Moreover, their design allows the investigation of many understudied aspects of ecology.

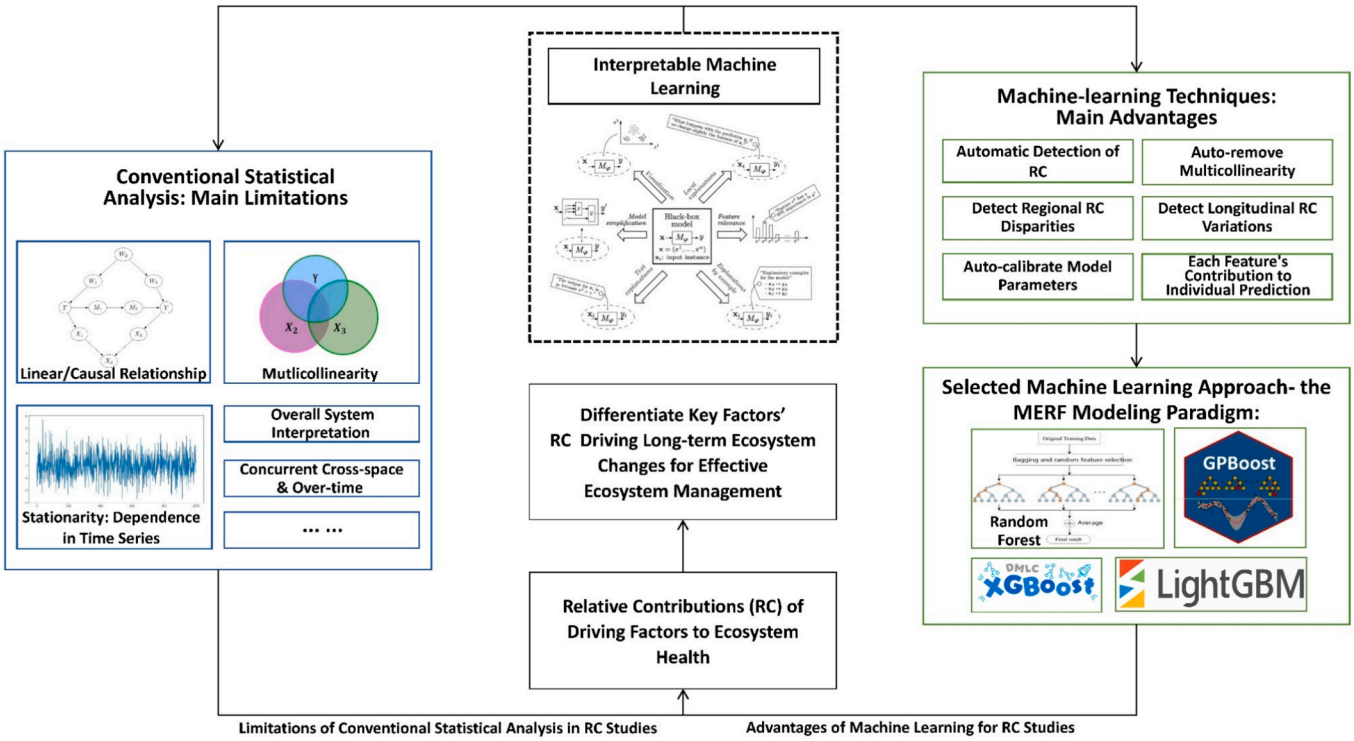

Fig. 1. The Conceptual Framework.

The ML approach has also been integrated to study the health of grassland ecosystems. For example, in the IMAR case study, Yang et al. (2024) integrated random forest (an ML technique), traditional regression, Theil-Sen estimation, Mann-Kendall trend analysis, and the geodetector models to estimate above-ground biomass (AGB) and to identify the driving forces affecting Inner Mongolia grassland AGB changes (Yang, 2024). Another random forest model was developed to simulate grassland productivity resistance to different climate extremes in temperate semi-arid grasslands of China (Huang et al., 2024). Parente et al. (2024) extracted more than 2.3 million samples based on visual interpretation of global time-series remote sensing images (Parente, 2024). They integrated these samples with multi-source static and dynamic environmental factors, including topography, climate, land surface temperature, and spatial distance information of cities and roads, to construct a probability prediction model of grassland classifications through spatiotemporal machine learning. Kladny et al. (2024) developed a convolutional long short-term memory (ConvLSTM) model to capture spatial and temporal dependencies in time series data, examining how different drought conditions impacted vegetation growth (Kladny et al., 2024). They demonstrated the accuracy of the deep learning model for predicting time series of ecosystem services under extreme environmental conditions.

Nevertheless, ML approaches in the eco-geo sciences are still rapidly developing, and their impact on the fields is limited. Current approaches to studying the RC of ESDF face several challenges. At first, most current ML-based explorations and applications focus on natural or physical processes (Parente, 2024; Zhou et al., 2022; Morueta-Holme et al., 2023; Hu et al., 2022; McCleery, 2023; Yang, 2024; O'Neill et al., 2018). Implementing ML approaches with eco-geo sciences must integrate with human dimensions, facilitate human interaction and interpretation (Hazeleger, 2024), adopt the open science principle (Bergen et al., 2019), and advocate multidisciplinary collaboration (Chen, 2024). The outcomes of ML-based models must be interpretable and understandable to concerned scientists, practitioners, and policymakers (Kaack, 2022). There is a call for developing interpretable MI (IML) models (Rudin, 2022, 2019). IML models are interpretable from the beginning instead of explaining ML predictions through post-process diagnostics (Irrgang, 2021). IML models are tightly hybrid between ML algorithms and conventional domain-specific models (Eyring et al., 2024).

Secondly, traditional statistical approaches often fail to handle linearity, multicollinearity, and the need for fine-grained (i.e., individual variable) interpretation. Many process-based models do not concurrently model spatial variations and time series dynamics. For example, econometric panel regression analysis (EPRA) and hierarchical linear mixed model (HLMM) can concurrently examine cross-space and time-series variations. However, EPRA and HLMM assume the existence of a linear relationship between the response variable and explanatory variables. They usually claim some causal relationships between the response variable and explanatory variables. The challenge is that linearity is seldom known or difficult to confirm in complex coupled human and natural systems (Schulz, 2020). Especially when datasets are extensive, multicollinearity is expected to exist in some pairs of explanatory variables. Multicollinearity occurs when two or more variables are highly correlated in a multiple linear regression model, making it challenging to interpret the regression outcomes. It is hard to handle multicollinearity in traditional statistical models. When the number of variables is large, PCA (principal component analysis) or some other form of dimensionality reduction is often recommended to transform a large number of variables into a set of fewer orthogonal features by using the covariance matrix (Yang et al., 2021). Reducing multicollinearity or shrinking dimensionality requires excellent statistical skills and domain knowledge.

Thirdly, process-based models lack a well-established approach for handling time series data. For example, Huang et al. (2024) assessed ecosystem health by incorporating a sustainable supply of ecosystem services from 2000 to 2020 (Huang et al., 2024). The paper selected a five-year time slot to examine temporal changes, rather than employing a continuous time series analysis. A five-year time slot was also employed by Lv et al. (2024) to examine the rapid shrub encroachment in grasslands from 1990 to 2020 in Inner Mongolia, China (Lv, 2024). Lu

Table 1
List of variables.

Short Name	Long Name	Unit
	Grassland Productivity as Proxy to Ecosystem Health[1]	
EVI	Enhanced vegetation index	Value range of –1 to + 1
	Climate Factors[2]	
Psum	Precipitation (summarized precipitation of each period in the growing season)	mm
Temp	Temperature (averaged temperature of each period in the growing season)	°C
	Socioeconomic Variables[3]	
Pp	Population density	1,000 per Km^2
Gp	Per capita gross domestic product (GDP)	1,000 Chinese Yuan
prpop	Percent of rural population to total population	%
iofp	Net income of farmers and pastoralists	Chinese Yuan
ls	the year-end number of livestock per square kilometer	1,000 head
gp	Grain production per square kilometers	ton
gova	the gross output value of farming, forestry, animal husbandry and fishery – share of GDP in a county	%
aa	percent of the arable area to total land area in a county	%
fai	fixed assets investment – share of GDP in a county	%
lgr	local government revenue – share of GDP in a county	%
lohsk	the total length of highways per square kilometers in a county	Km/Km^2
HMP	health & medical professionals per ten thousand people in a county	person/10,000 people
HPB	hospital beds per ten thousand people in a county	bed/10,000 people
MHT	middle & high school teachers per ten thousand people in a county	person/10,000 people
PTE	professional & technical employment per ten thousand people in a county	person/10,000 people
Pcurei	per capita disposable income of permanent urban residents in a county	1000 Yuan pc
PIO	primary industry output value – share of GDP in a county	%
SIO	secondary industry output value – share of GDP in a county	%
TIO	tertiary industry output value – share of GDP in a county	%
TCRV	total consumer retail value – share of GDP in a county	%
	Land Use Types[4]	
Grass	grassland area (percentage to total land area)	%
CropPG	crop area + planted grassland for harvest (percentage to grassland)	%
Urban	urban area (percentage to total land area)	%
Wateru	water area (percentage to total land area)	%
	Environmental and Technology Factors[5]	
dustgdp	GDP per unit discharge of industrial dust	1,000 Yuan
fosgdp	GDP per unit area of forest land	1,000 Yuan
interp	Internet users per capita	Int. Users/1,000 people
invpa_p	Invention patent applications per capita	Patent applications/ 1,000 people
mobile_p	Mobile phone per capita	Buses/1,000 people
noxgdp	GDP per unit nitrogen oxide emission	1,000 Yuan
road_p	Road area per capita	Km
sdxgdp	GDP per unit sulfur dioxide emission	1,000 Yuan
bus_p	Bus per capita	Buses/1,000 people
taxiv	Taxi per capita	Taxis/1,000 people
telev	Telecom business volume per capita	Telecom sets/1,000 people

et al. (2023) integrated a suite of tools, including the Hurst index, correlation analysis, coefficient of variation, gravity center model, and wavelet analysis, to investigate the spatial and temporal changes in vegetation net primary productivity and its driving factors (Yuan, 2023). Gong et al. (2024) employed the land surface water index, vegetation photosynthesis model, and linear regression to explore the spatiotemporal dynamics of gross primary productivity and its driving mechanism in the Loess Plateau, China (Gong et al., 2024). These studies coupled spatial and temporal analyses, rather than providing a systematic framework for examining spatiotemporal dynamics concurrently, as EPRA and HLMM do. These studies conducted temporal analysis, but not a time series analysis of how past conditions affected recent states.

In this study, we analyze the limitations of current statistical approaches to studying the relative contribution (RC) of ecosystem sustainability driving factors (ESDF) (Fig. 1), investigate which machine-learning techniques are suitable for differentiating the RC of ESDF, and illustrate unique contributions of IML solutions through a case study of grassland ecosystem health in the Inner Mongolia Plateau. The scientific and methodological contributions include (1) identifying ML methods that can explicitly and concurrently examine spatial and time-series (spatiotemporal) variations and dynamics of ecosystem health, (2) breaking several limitations of traditional statistical and process-based models, (3) incorporating a large set of socioenvironmental variables to examine anthropogenic impacts on ecosystem health, (4) robust feature engineering to identify RC of important ESDF, (5) fine-grained interpretation of each feature's contribution to individual prediction (EFCTIP), and (6) localized EFCTIP.

2. The study area, data, and methods

2.1. The study area and data

Grassland is an essential element of the terrestrial ecosystem (Li et al., 2023), accounting for about 1/3 of global terrestrial vegetation covers (Gong et al., 2024). Grasslands provide crucial ecosystem services, such as food production and habitats for organisms (Boukari, 2019). Most grasslands are in semi-arid, arid, and semi-humid areas. Humans have exploited these areas for a long time, and global climate changes are most noticeable in such regions (Shiferaw et al., 2025). For example, the Inner Mongolia Autonomous Region (IMAR) is located on the northern border of China and the southern part of the Mongolia Plateau. IMAR is the main distribution area of temperate grasslands in China, accounting for about 67 percent of the region's total area and 22 percent of the grassland area of China. Rapid economic development and population increase have led to intensive grazing, farming, mining, and urbanization in IMAR, which makes IMAR an excellent case to study how these socioeconomic and LULC drivers and climate change affect grassland productivity (Koppa et al., 2022).

The case study datasets contain 38 variables, of which EVI (enhanced vegetation index, a proxy of grassland productivity) is the target variable (Table 1). The covariates include two climate factors, four LULC types, 11 environmental and technological indicators, and 20 socioeconomic variables covering 67 counties from 2001 to 2018. This dataset is extensive in terms of broad inclusion of socioeconomic and environmental factors for examining their interactions with grassland ecosystem health. The separation of the variables into different categories is based on the scopes and sources of the data. The source data for EVI, precipitation, and temperature are contained in raster images with a 250 m resolution. The LULC raster datasets are at 500 m and 30 m resolutions. Since the final analysis unit is the county, all data are resampled as mean values within county boundaries. In addition, all variables are standardized as Z-scores. Finally, both environmental and socioeconomic data are organized as an across-space and time-series panel dataset to support concurrent spatiotemporal analysis.

(a) The response variable is the enhanced vegetation index (*EVI*), a better proxy of grassland productivity in the study area (Li and Xie,

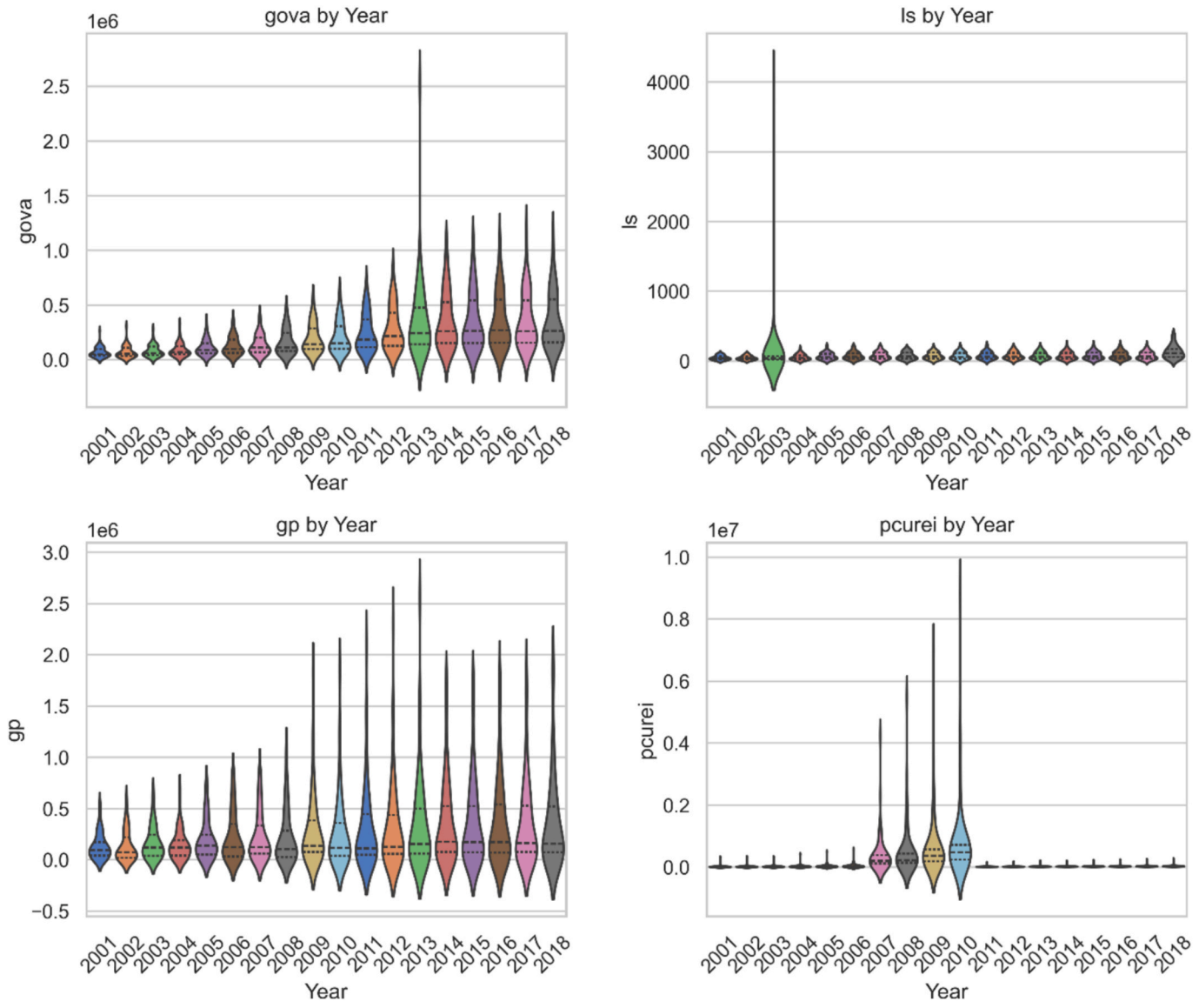

Fig. 2. Distribution characteristics of four indicators on agriculture, grazing, and urban income.

2013). *EVI*'s source is the MOD13Q1 product (Li, 2013), with 250 m spatial resolution and 16-day temporal resolution over the growing season (9 May to 29 September) for 18 years from 2000 to 2017.

(b) Two climatic factors, precipitation (*PRE*) and temperature (*TEM*) were collected from 50 weather stations across IMAR (https://cdc.cma.gov.cn). Those climate variables were spatially interpolated as the grid maps at 250 m × 250 m using ArcGIS Inverse Distance Weighted (IDW) interpolation adopted from the work of Chen and his colleagues (Price et al., 2000). Daily precipitations were added as 16-day sums while daily average temperatures were averaged as 16-day averages.

(c) The socioeconomic variables were collected from the IMAR statistic yearbooks 2000–2017 published by IMAR Statistical Bureau (2001–2018) (IMAR, 2017). The socioeconomic, environmental and technological data are yearly statistics. The socioeconomic data were normalized according to GDP, total area, and total population. For instance, GPD and rural populations were normalized by the total population as *gdppc* and *srural*. The units were per capita and the share or percentage, respectively. The arable area, grain production, length of highway, and livestock were standardized by the total area as the density indicators (*daa*, *dgr*, *dhw,* and *dls*). The farmer and pastoralist income, farming income, local government revenue, and governmental investment were standardized by GDP as the share of GPD, *sfinc*, *sfarm, slgov*, and *sinv*.

(d) The data of LULC primarily came from The NASA MCD12Q1 Data Product (https://lpdaac.usgs.gov/products/mcd12q1v006/) at 500 m resolution. 16 out of the 17 International Geosphere-Biosphere Program LULC types were found in the study area, except "Evergreen Broadleaf Forest" (https://www.igbp.net/). However, the urban land areas in the NASA MCD12Q1 Data Product were the values in 2000 and no further updates were provided. Therefore, the urban land data was replaced with the impervious land surface dataset of China (Gong et al., 2019).

(e) Patent data is mainly derived from the patent cloud website (https://app.patentcloud.com/), and the environmental and technological data are mainly from the Online China Urban Statistics Yearbook (https://data.cnki.net/yearbook/Single/N2020050229). Seventeen out of 84 counties are primary grazing economies and didn't report environmental pollution data. They were excluded from the study.

Violin plots (a combination of box plot and density plot) were produced for all variables to analyze data distribution characteristics. Due to the large number of variables, several unique ones were presented and explained in the main text (Figs. 2 and 3), while the remaining ones are provided in the Supplementary Document. For example, *Gova* (the gross output of farming, forestry, animal husbandry, and fishery) gradually increased annually from 2001 to 2018, showing a general trend of

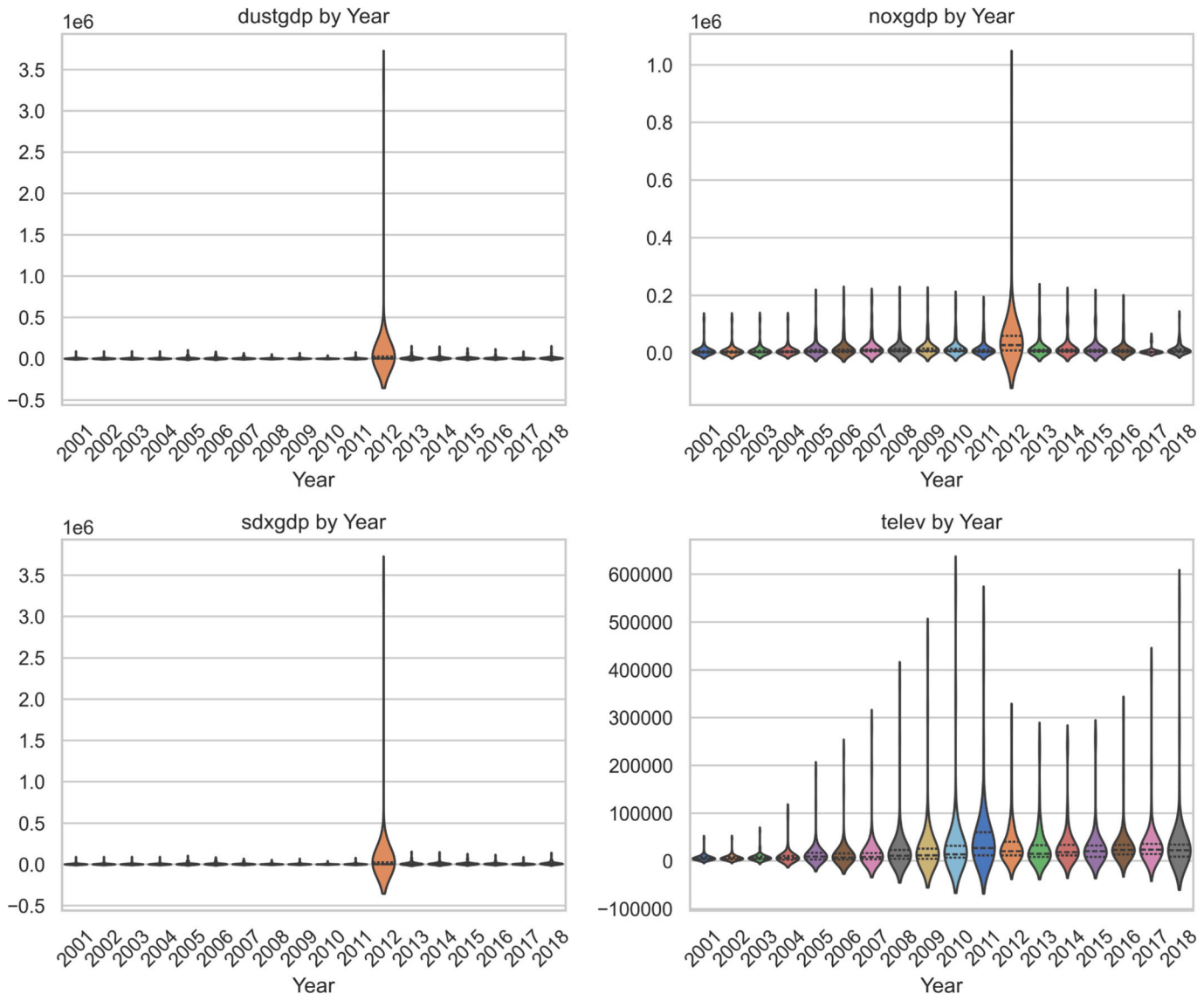

Fig. 3. Distribution characteristics of environmental pollution, telecom, and wetland indicators.

socioeconomic variables. However, *Gova* displayed an abnormal phenomenon in 2013. In the spring of 2013, the central and western regions of Inner Mongolia experienced low precipitation and high temperatures, resulting in widespread droughts (China Meteorological Administration, 2013). Droughts in Ordos City, Baotou, and many other places in the west and central regions were more severe, which led to a decrease in *Gova*.

Ls (the year-end number of livestock per square kilometer) was unusually high in 2003. The central government of China accelerated the policy of returning grazing land to grassland in 2003, which led to a more comprehensive and detailed counting of the number of livestock at the end of the year (State Council Gazette, 2013). The values of *gp* were higher in 2008–2009. The Chinese government increased the total amount of agricultural subsidies by at least 20 percent from the previous year in 2008. The Chinese government also implemented comprehensive support measures, such as direct payments, price support, preferential credit, and tax exemptions for grain production in the following years, which led to noticeable jumps of *gp* (Information Office of the Ministry of Agriculture, 2011).

Pcurei (per capita disposable income of permanent urban residents) showed unusually high values during 2007–2011. Inner Mongolia's economy has long relied on mining commodities, such as coal and rare earths. Productions in these sectors expanded rapidly between 2008 and 2011, but then global commodity prices fell sharply since 2011, leading to a narrower increase in corporate profits and workers' wages (Central Government Gate, 2015). Furthermore, macroeconomic control cooled down these sectors. In addition, rural migrants to cities were counted as "urban population" since 2012, lowering the average *Pcurei* value but more truly reflecting the changes in the income structure in the process of urbanization.

Three environmental pollution indicators, *dustgdp, noxgdp*, and *sdxgdp*, experienced a significant increase in 2012 (Fig. 3). As discussed above, Inner Mongolia's economy heavily depended on coal and rare earth mining and witnessed rapid expansion from 2008 to 2011. By 2012, the added values of these industries in Inner Mongolia increased by 14.8 %, much higher than the per capita GDP growth rate, reflecting that the regional economy was still highly dependent on the development of resource-based industries (Central Government Gate, 2015). Driven by the "Twelfth Five-Year Plan", Ordos, Wuhai, Baotou, and other areas vigorously developed the coal chemical industry and extended the coal industry chain, including coal-to-liquid, coal-to-olefins, and other projects, which further exacerbated these pollution indicators.

Telev (tele-communication growth) was booming from 2007 to 2011

Algorithm 1 GPBooster: Explicit Definition of Cross Sections and Time Series

Input:

1. Input Data Structure Example:

- `xdata`: Input feature data with columns:
  `ID, Year, CID, Psum1, Temp1, Pp1, ...`

ID	Year	CID	Psum1	Temp1	Pp1
0	2001	81	-1.645	0.886	...
1	2001	2042	-0.554	1.325	...
2	2001	871	0.015	0.763	...
⋮	⋮	⋮	⋮	⋮	⋮

- `y`: Target variable with columns: `ID, EVI1, Notes`

ID	EVI1	Notes
0	0.253	ID-Dataset Index
1	0.393	Year-Time Index
2	-0.072	CID-County Index
⋮	⋮	⋮

2. Read input files

xdf ← pd.read_csv(xdata).drop(ID, axis = 1)
y ← pd.read_csv(y).drop(ID, axis = 1)

3. Split training and testing datasets

X_train, X_test, y_train, y_test ← train_test_split(xdf, y, test_size = 0.30)

4. Merge Year and CID into Space-Time Group Object

Year_train ← X_train[Year]
Year_test ← X_test[Year]
CID_train ← X_train[CID]
CID_test ← X_test[CID]
group_train ← pd.concat([Year_train, CID_train], axis = 1)
group_test ← pd.concat([Year_test, CID_test], axis = 1)

5. Fit GPBooster model

model ← gpb.GPModel(group_data = group_train)
model_instance ← model
data_train ← gpb.Dataset(X_train, y_train)
bst ← gpb.train(params, data_train, model_instance)

Note: Params configuration is omitted in this pseudocode.

Fig. 4. Pseudocode for GPBooster explicitly defines the cross sections and time series.

as well. The Ministry of Industry and Information Technology (MIIT) of China successively approved the 3G licenses of the three biggest telecom operators in China, and immediately launched large-scale network construction and user promotion. Following the launch of 3G network coverage, mobile data and multimedia services (such as video calling and mobile office) experienced rapid growth, leading to a significant increase in business volume from 2010 to 2011. In 2010, the State Council unveiled the "Broadband China" action plan, which clearly stated the goal of "accelerating the construction of urban optical networks and rural broadband." Broadband access costs have decreased, bandwidth has increased significantly, and Internet usage has skyrocketed among both home and business users (Network, 2009).

2.2. Newly developed interpretable machine-learning algorithms

Big data analytics are particularly effective when nonlinear relationships exist (Schulz, 2020) or when many variables need to be trained to shrink dimensionality or remove multicollinearity (Bruce and Bruce, 2017). More importantly, machine-learning techniques encompass many computational algorithms, support automatic feature engineering (dimensionality reduction and multicollinearity removal) and automatic calibration of model parameters, provide flexible ways of visualizing model training and testing processes and outcomes, and enable analysts to incorporate their expert knowledge to interpret and validate data, models, and findings. These new capacities of machine-learning techniques can break the limitations confronted by traditional statistical methods.

Table 2
The summary statistics of the EPRA and the HLMM models.

The EPRA Model			
Fixed-effects (within) regression	Number of obs	=	1,156
Group variable: ***CID***	Number of groups	=	68
R-sq:	Obs per group:		
within = 0.2083	min	=	17
between = 0.0036	avg	=	17
overall = 0.0021	max	=	17
	F(25,1063)	=	11.19
corr(EVI, Xb) = -0.2110	Prob > F	=	0
The HLMM model			
Mixed-effects regression	Number of obs	=	1,156
Group variable: ***CID***	Number of groups	=	68
R-sq:	Obs per group:		
0.1623	min	=	17
corr(EVI, Xb) = 0.4029	avg	=	17
	max	=	17
	Wald chi2(25)		543.10
	Prob > chi2		0.00
	Log pseudolikelihood		−441.72
Mixed-effects regression	Number of obs	=	1,156
Group variable: ***Year***	Number of groups	=	17
R-sq:	Obs per group:		
0.5974	min	=	68
corr(EVI, Xb) = 0.7729	avg	=	68
	max	=	68
	Wald chi2(16)		.
	Prob > chi2		.
	Log pseudolikelihood		−1097.89

Table 3
Summary of Statistics of Four Machine-learning Gradient Boosting Models.

GPBoost	Mean Squared Error	0.1192
	R-squared	0.8807
XGBoost	Mean Squared Error	0.2876
	R-squared	0.7179
LightGBM	Mean Squared Error	0.5124
	R-squared	0.4875
MERF	Mean Squared Error	0.1411
	R-squared	0.8588
MERF-XGBoost	Mean Squared Error	0.1133
	R-squared	**0.8866**
MERF-LightGBM	Mean Squared Error	0.1211
	R-squared	0.8789
MERF-GPB	Mean Squared Error	0.1254
	R-squared	0.8746

We focus on solving the limitations that conventional EPRA, HLMM, and process-based models face, such as linearity, multicollinearity, and the need for fine-grained analysis. Notably, quantifying and differentiating relative contributions (RC) of ecosystem sustainability driving factors (ESDF), such as climate, environmental, and socioeconomic factors, are crucial for effective ecosystem management. RC studies of ESDF must consider three unique features. Ecosystems are complex coupled human-nature systems that consist of almost all earth subsystems and many socioeconomic and policy elements and necessitate examinations of correlations, covariations, and causal structures among a large set of variables (Kline, 2023). For this reason, this research has compiled a comprehensive dataset on environmental and socioeconomic aspects to support this study. Secondly, predicting future ecosystem health must understand the present conditions and the past evolutionary dynamics (Bergen et al., 2019). Thirdly, ecosystems display evident spatial heterogeneity, which becomes typical characteristics of ecosystem diversity and resilience (Xie et al., 2021). Therefore, we must simultaneously examine spatial and temporal changes and dynamics of complex interactions and feedback embedded in a coupled socio-ecological systems (Xie, 2023). In other words, this research intends to

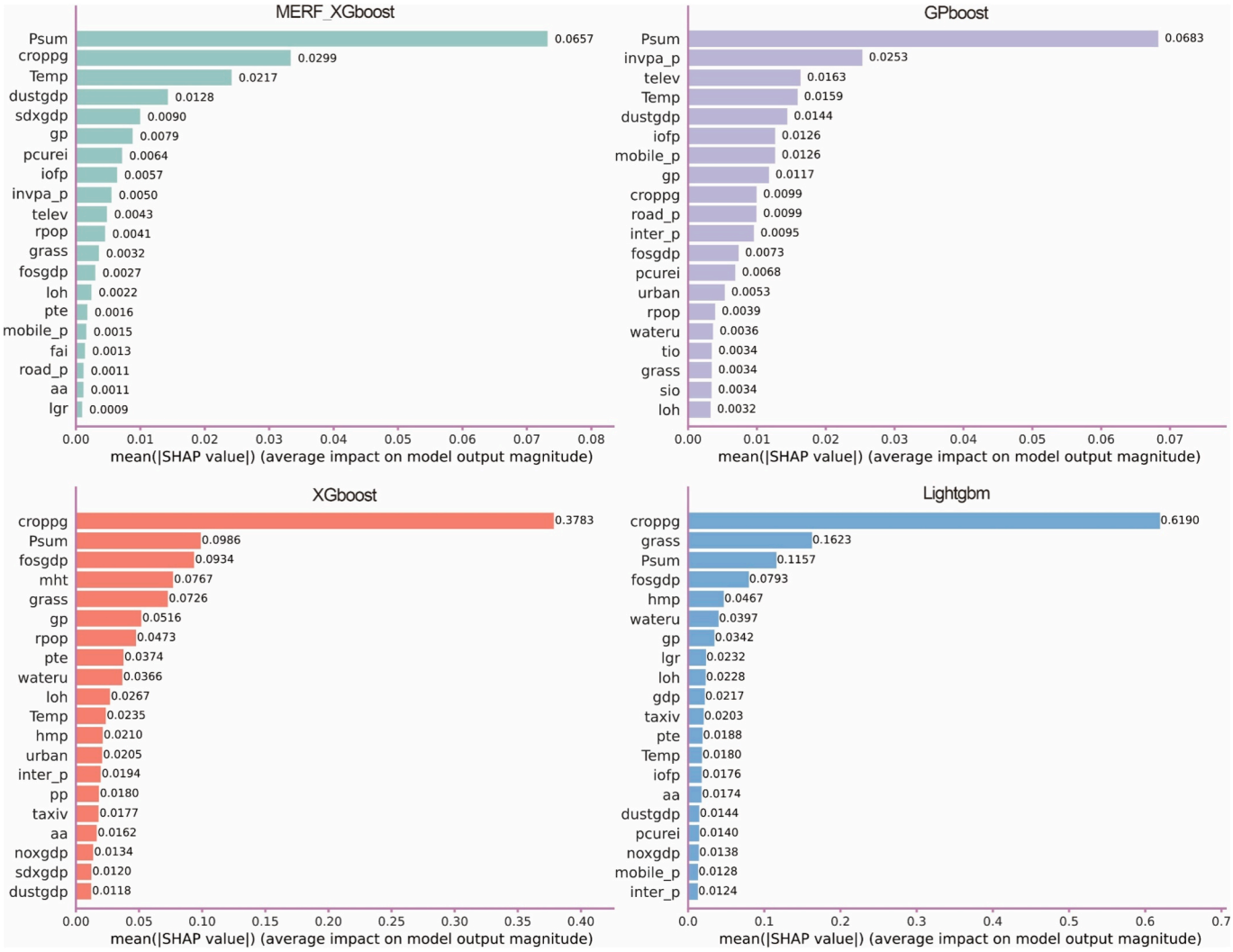

Fig. 5. The Determination of Important Features Contributing to Grassland Productivity*. *SHAP is an abbreviation of Shapley Additive exPlanations. The concept of SHAP values comes from cooperative game theory. The contribution of each feature to a prediction should be calculated as the average marginal contribution of that feature across all possible feature combinations. Therefore, SHAP values are local, additive feature attributions that quantify how much each feature contributes to a single prediction relative to a baseline. Rather than giving one global importance score per feature, SHAP computes for each case and each feature the signed contribution that feature makes toward pushing the model's output above or below a reference value (e.g. the mean prediction). In practice, this means that when the model makes a prediction for a particular observation, its SHAP values indicate both which features drove the prediction and by how much they contributed to moving it in the positive or negative direction. Summing all SHAP values (plus the baseline) exactly recovers the model's output for that case. In other words, when the model makes each prediction, SHAP values can tell us which features are the most important to the prediction and how much they contributed to it.

identify machine-learning algorithms that can explicitly handle panel data (cross-section and time series data, also called grouped data or longitudinal data). Panel data has a unique structure. It is multidimensional (i.e., cross-sectional), indexed by Section ID or Case ID (Xie, 2023). The data structure is also a time series, indexed by Time ID. In other words, panel data has a 3D data structure, explicitly considering both space and time simultaneously. An execution of a panel data analysis requires an explicit declaration of the Section ID and Time ID (Fig. 4). Through a thorough examination, we have found four viable machine-learning algorithms that can handle panel data: Mixed Effects Random Forest (MERF), eXtreme Gradient Boosting (XGBoost), Gaussian Process Boosting (GPBoost), and Light Gradient Boosting Machine (LightGBM). Although these models are well-established ML approaches and frequently adopted in grassland ecosystem research (Jia et al., 2024; Zhang, 2022), their capabilities of examining spatiotemporal dynamics simultaneously are not fully illustrated. This research fills this gap, which is one of the novelties of this paper.

It is worth pointing out that geographically weighted regression (GWR) models are powerful tools for examining spatially varying relationships in great detail (Shrestha, 2024; Su et al., 2017), although they are not designed to explore time series changes. GWR can generate a set of local-specific coefficients, including individual R-sq, parameter estimates, and corresponding *t*-test values. These local-specific coefficients can be mapped to interpret spatially varying relationships between the dependent and independent variables (Li et al., 2021). Several GWR models were performed for comparison.

2.2.1. *MERF*

MERF model combines the random forest and mixed effects models. MERF, like GPBoost, explicitly constructs datasets into cross-section (space) and over-time (time) panels (Fig. 4). It is designed to address problems with hierarchical data, such as longitudinal studies or data with a group structure. In the MERF model, the random forest handles heterogeneity and non-linear relationships between groups (Tan et al., 2023). In contrast, the mixed effects model models correlations and random effects within groups. This combination allows the model to account for the hierarchical structure of the data and correlations between groups, thereby enhancing its ability to model complex data and

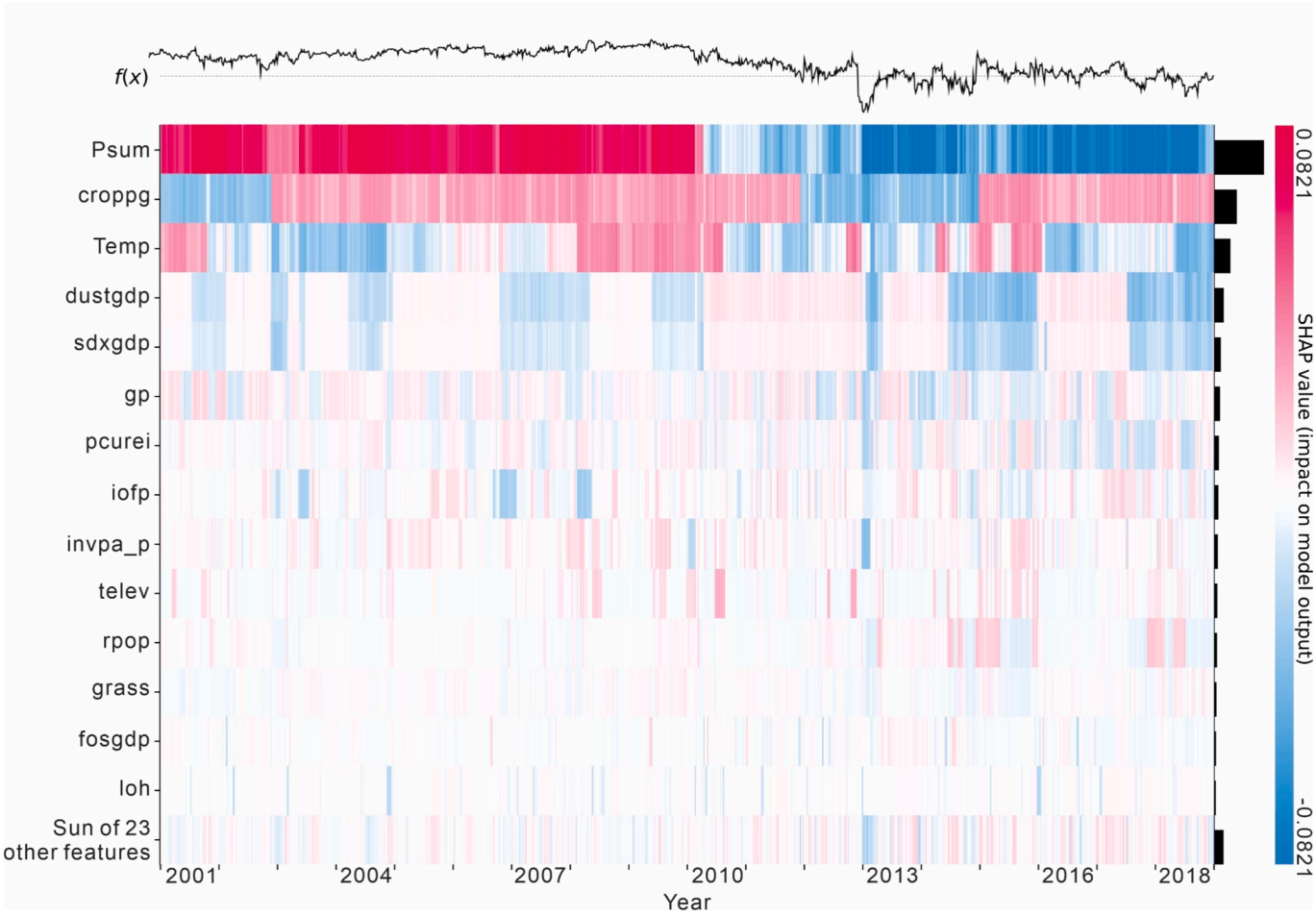

Fig. 6. The Heatmap of SHAP values between the test period, 2001 – 2018*. * The y-axis displays significant covariates based on their SHAP values. The x-axis lists the cases by observation years.

handle imbalanced datasets and missing values. Through this combination, the MERF model is better suited for adapting to data with hierarchical or clustered structures, such as longitudinal panel data or spatial data.

The following are the basic principles of the MERF model:

$$y_i = f(X_i) + A_i \cdot b_i + e_i \tag{1}$$

where:y_i is the $n_i \times 1$ vector of responses for cluster *i*. X_i is the $n_i \times p$ fixed effects covariates that are associated with the y_i. A_i is the $n_i \times q$ random effects covariates that are associated with the y_i. b_i $N(0, D)$ is the $n_i \times 1$ vector of errors for cluster *i*. *i* is the cluster ID. e_i is the $n_i \times 1$ vector of errors and is assumed to be completely random across all clusters.

Furthermore, MERF is a flexible machine-learning platform. The fixed effect, $f(X_i)$, can be solved by various algorithms, such as XGBoost, GPBoost, and LightGBM. This is MERF's biggest advantage over other machine-learning algorithms. Therefore, we integrate the longitudinal structured data and EPRA analytical processes with the MERF family models to create an interpretable ML models. We focus on the classic challenges EPRA and HLMM face and the new insights the MERF-family models can achieve. These new insights include but are not limited to the automatic detection of relative contributions (ADRC) of important biophysical and socioeconomic factors on grassland productivity; the fine-grained visualization of spatiotemporal patterns of RC variations across counties and over the years; visualization and local analysis of each feature's contribution to individual prediction (EFCTIP); and automatic calibration of model parameters (ACMP). These advantages facilitate researchers in understanding complex interactions between ecosystem health, climate change, LULC, and socioeconomic transformation. They affect how we model RC of biophysical and socioeconomic factors to ecosystems and become promising paradigms for studying change dynamics and interactions embedded in coupled human-natural systems.

2.2.2. Xgboost

XGBoost is a foundational algorithm of the optimized gradient boosting-tree family and is closely related to GPBoost and LightGBM. XGBoost can be used for both classification and regression tasks. It enhances predictive performance by combining multiple weak learners (typically decision trees) into a strong learner. It achieves high performance through block-wise feature splitting, cache awareness, and parallel processing to improve training speed and model performance (Chen and Guestrin, 2016; Fu et al., 2019). During training, XGBoost utilizes gradient descent to optimize model parameters, making it capable of handling high-dimensional sparse features, missing values, and nonlinear relationships while exhibiting robustness and generalization ability.

The objective function of XGBoost, which measures the model's fit to the training data and its complexity, can be expressed as follows:

$$Obj = \sum_{i=1}^{n} loss(y_i, \hat{y}_i^{(t)}) + \sum_{k=1}^{t} \varepsilon(f_k) \tag{2}$$

where:$loss(y_i, \hat{y}_i)$ represents the loss function, which measures the discrepancy between the predicted $\hat{y}_i$ and the true label y_i. $\varepsilon(f_k)$ repre-

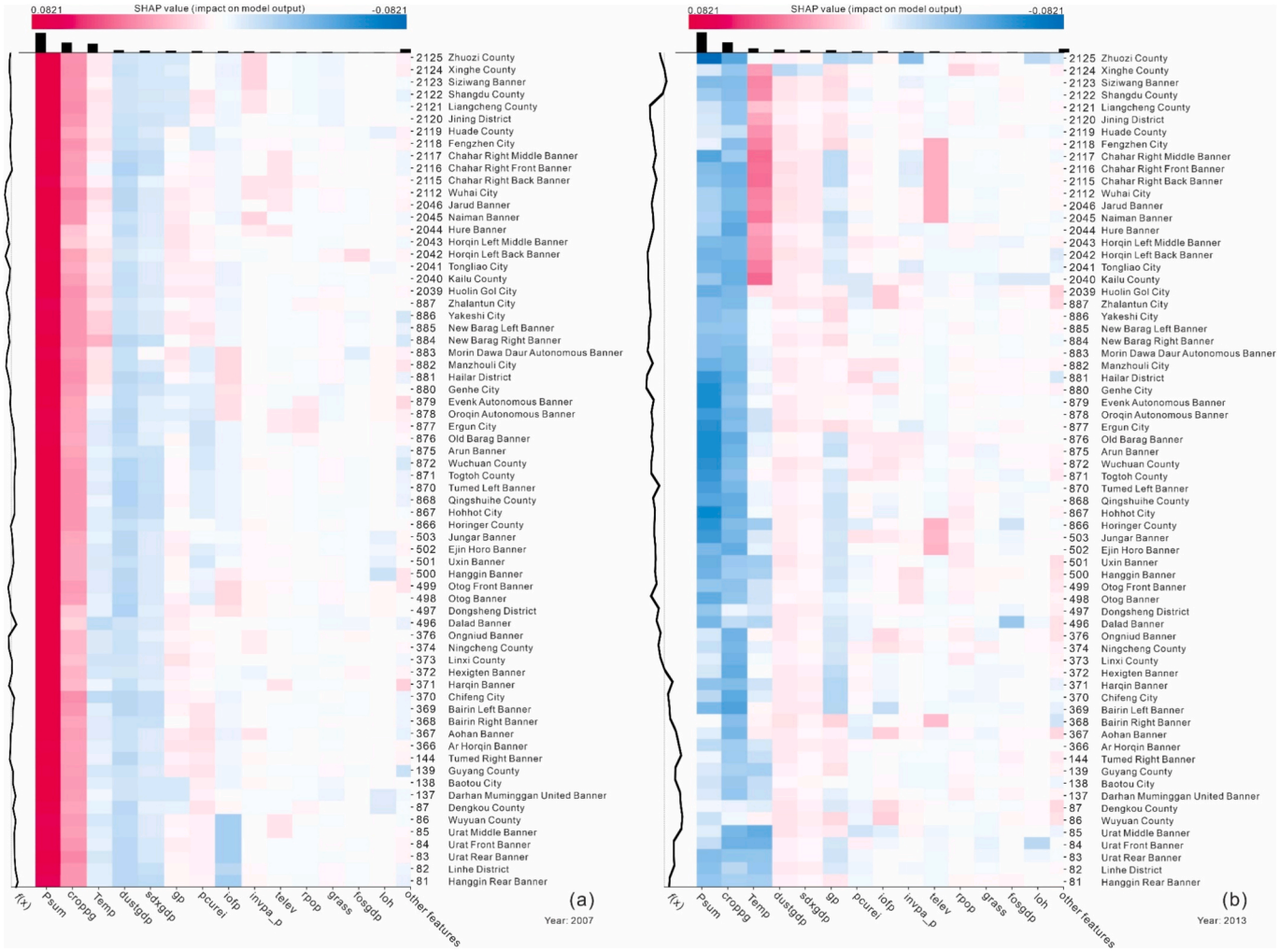

Fig. 7. (a) The Heatmap of Important Features in 2007, (b) The Heatmap of Important Features in 2013.

sents the regularization term, controlling the model's complexity to prevent overfitting. t represents the step so $\hat{y}_i^{(t)}$ means the prediction value at step t. f_k denotes the k th weak classifier.

XGBoost excels in handling structured data and nonlinear relationships, commonly applied in regression and classification tasks (Celbiş et al., 2023). Additionally, it offers functionalities such as feature importance assessment and visualization, early stopping, and cross-validation to assist users in optimizing models and avoiding overfitting. This paper integrates the XGBoost algorithm with the MERF modeling framework (MERF-XGB), generating the highest R-sq value. The paper also experimented with the GPBoost and the LightGBM algorithms for comparison.

2.2.3. Gpboost

GPBoost combines tree-boosting with Gaussian process and grouped random effects models. It supports independently applying tree-boosting, Gaussian process, and (generalized) linear mixed effects models (LMMs and GLMMs). GPBoost explicitly considers a panel data structure with both spatial and temporal indices through a concatenation function (Algorithm 1). GPBoost is a machine learning framework specifically designed to handle large-scale data and high-dimensional features (Sigrist, 2022). It was developed based on XGBoost and incorporates the concept of Gaussian processes. It can be seen as a synthesis of three modeling frameworks, traditional (generalized) linear mixed effects, Gaussian process models, and classical independent tree-boosting algorithms.

GPBoost algorithm assumes that the response variable Y is the sum of a potentially non-linear mean function $\Omega(X)$ and random effects Zb:

$$Y = \Omega(X) + Zb + x_i \tag{3}$$

where: $\Omega(X)$ is an ensemble of trees, X are predictor variables (aka covariates or features), and x_i is an independent error term. Zb represents the random effects and can consist of Gaussian processes (including random coefficient processes) and grouped random effects (including nested, crossed, and random coefficient effects).

Compared to traditional (generalized) linear mixed effects and Gaussian process models, GPBoost algorithm can establish fixed effect function models in a non-parametric and non-linear manner, building more realistic models and achieving higher prediction accuracy. Compared to classical independent boosting algorithms, GPBoost introduces Gaussian processes to model the uncertainty of the model, enabling more effective learning of prediction functions and improving prediction accuracy. It can efficiently model high-cardinality categorical variables as well as spatial or spatio-temporal data. GPBoost excels in handling sparse data, large-scale datasets, and high-dimensional features, demonstrating high predictive performance and good interpretability.

2.2.4. LightGBM

LightGBM is a high-performance machine learning algorithm based on the gradient boosting framework. It employs a histogram-based decision tree learning algorithm, which discretizes continuous features

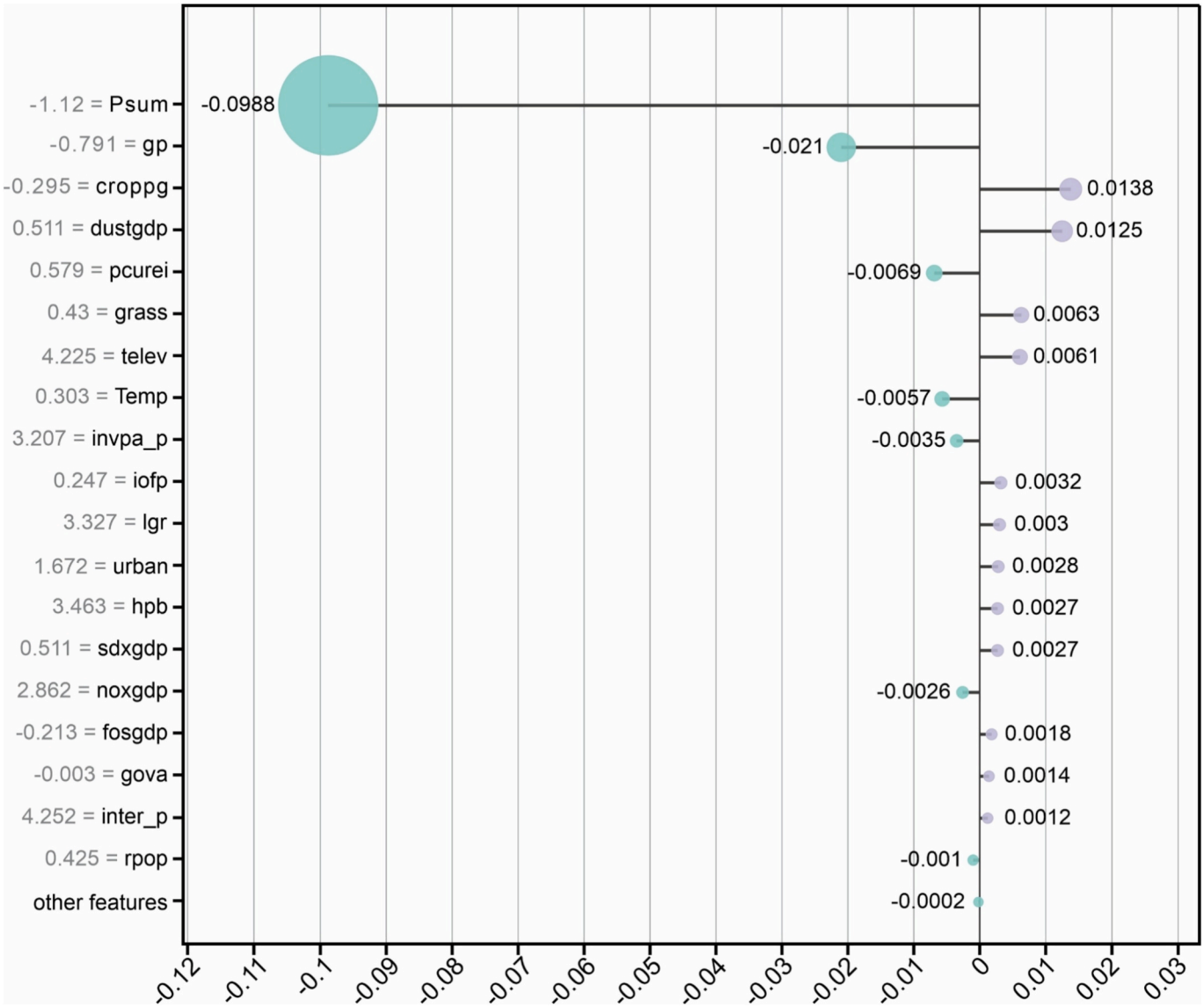

Fig. 8. Local SHAP Value Bar of Ejina Banner in 2018.

into discrete histograms to enhance training speed and memory efficiency. Additionally, it utilizes histogram-based decision tree algorithms and exclusive feature bundling to improve training speed and model performance further (Ke, 2017). LightGBM has achieved significant success in many data science competitions and real-world projects due to its ability to handle large-scale datasets, high-dimensional features, and imbalanced datasets while maintaining high predictive performance and low computational costs (Meng, 2016).

2.2.5. *Geographically weighted regression model*

The GWR model can be formulated as Gao and Li's research (Gao and Li, 2011):

$$y_i = \beta_o(g_i, h_i) + \sum_k \beta_k(g_i, h_i)x_k + \varepsilon_i \quad (4)$$

where y_i is the dependent variable at location i, $\beta_o(g_i, h_i)$ is the intercept at location i, (g_i, h_i) denotes the coordinates of location i, $\beta_k(g_i, h_i)$ is the local parameter estimate of independent variable x_k at location i, and ε_i denotes the random error term for location i.

3. Results and discussion

3.1. *The classic challenges EPRA and HLMM face*

For EPRA and HLMM, we must assess multicollinearity, stationarity, and fixed or random effects. Based on conventional exploratory statistical analysis, we produced a correlation matrix and conducted a very important feature (VIF) test to assess multicollinearity interactively. We removed those variables that had both higher VIF values and correlation coefficients. As a result, 13 variables were removed, and 25 were kept for further analysis (A-Table 1). Next, we performed the Levin–Lin–Chu (LLC) test to see whether a unit root or stationarity exists in those 25 variables. The LLC unit root test assumes that the time series contains a common unit root; the alternative is that this series is stationary (Levin et al., 2002). If a unit root was found, we adopted either the Differencing or Lag method to remove it (A-Table 2) (Xie, 2023). We then conducted the Hausmann test to assess which type of estimation an EPRA model should apply: a fixed-effect model or a random-effect model (Baltagi, 2004). The Hausmann test suggested an EPRA fixed-effect model with the explanatory variables that passed the multicollinearity test and underwent the unit-root removal (A-Table 3). Meanwhile, for an HLMM model, we tested both cross-sections (the county index – *CID*) and time-

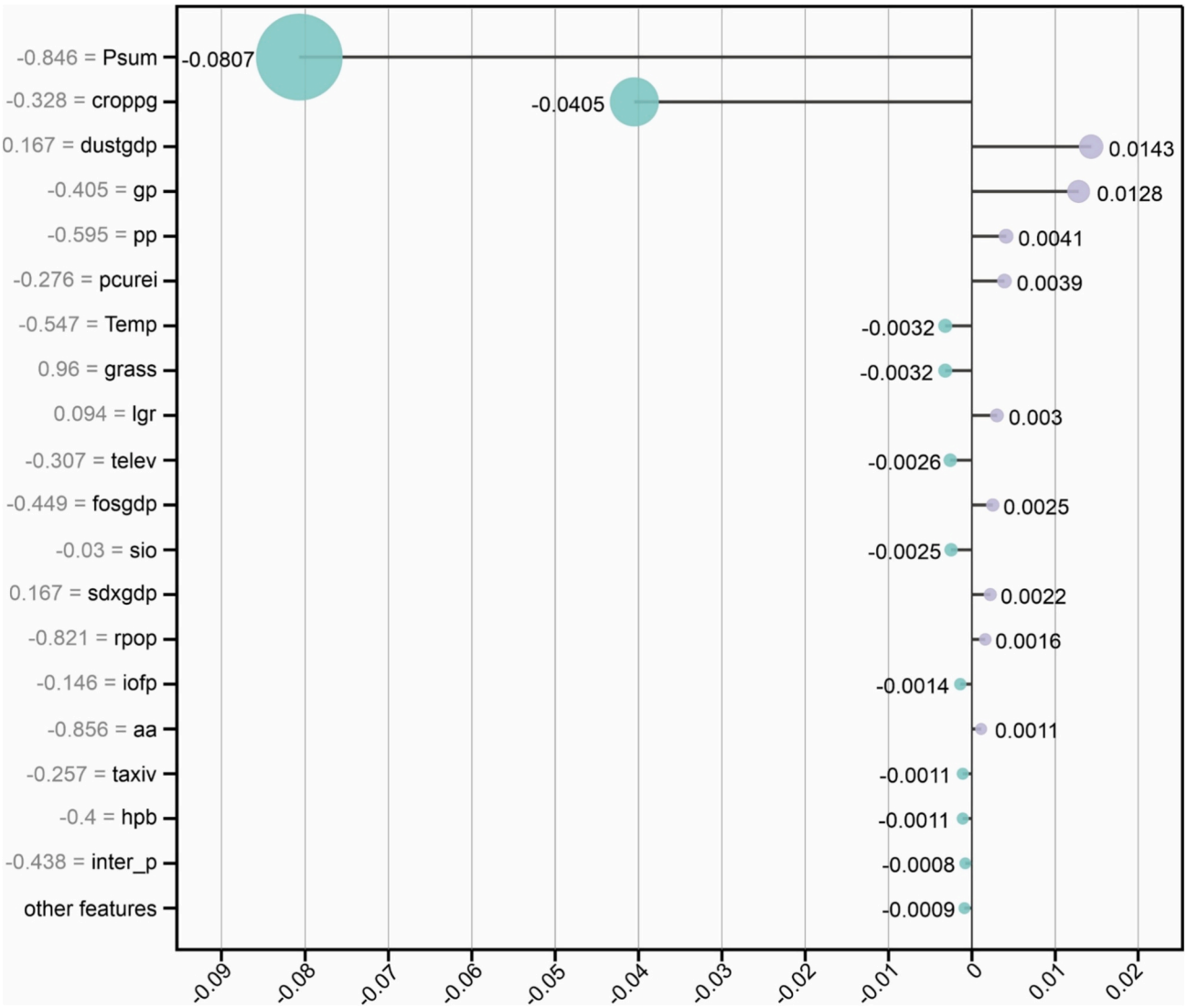

Fig. 9. Local SHAP Value Bar of Baotou City in 2018.

series (*Year*) as the grouping variables, revealing the random effect (Lu et al., 2024).

The summary statistics of the EPRA and HLMM models are reported in Table 2. The model coefficients and related statistics are reported in A-Table 4, 5, and 6. The R-sq. values were very low for the EPSA model (overall R-sq. = 0.0021) and for the HLMM model with *CID* (Counties) as the group variable (R-sq. = 0.1623). These findings indicated that the EPSA model and the HLMM-CID model were unsuitable for revealing relationships between *EVI* and the other climate, LULC, and socio-environmental drivers. Therefore, these two models could not assess the RC of biophysical and socioeconomic variables to ecosystem health or be suitable for estimating or predicting *evi*. However, the HLMM model with *Year* as the group variable obtained a moderate R-sq. value (=0.5874). Since the time series (*Year*) was short (17), each year had 68 cases (Table 1). As a result, the performance of the HLMM-Year model was much better than the HLMM-CID model but not compatible with the outcomes of most IML models.

3.2. Automatically Detecting RC of Climate, LULC, and socioeconomic covariates

Four models, GPBoost, XGBoost, LightGBM, and MERF, were reported in this section. Additionally, the MERF modeling framework can integrate several gradient boosting algorithms, including XGBRegressor, GPBoostRegressor, and LightGBMRegressor. As a result, the outcomes of these seven models were included in Table 3. The combination of MERF-XGB (Regressor) produced the highest R-sq (0.8866) among these ML algorithms that can handle space–time structured data (Table 3). The GPBoost model also achieved a very good R-sq, 0.8807. The models of MERF, MERF-LightGBM, MERF-GBM, and XGBoost got R-sq values between 0.72 and 0.88. Even LightGBM achieved a moderate R-squared value of 0.49. Compared with the EPRA model and the HLMM model with *CID* as the group variable, many more variables made essential contributions to the response variable, *EVI*, grassland productivity, and the R^2 values from the ML models were dramatically raised.

The most noticeable advantage of ML models is the automatic identification of biophysical and socioeconomic covariates that significantly contribute to ecosystem health. This process is also called feature engineering, which automatically removes multicollinearity and identifies important features contributing to the prediction of the response variable. The important features resembled each other to some degree between the models of MERF-XGB and GPBoost, as well as between XGBoost and LightGBM (Fig. 5). We chose the MERF-XGB model as an illustration for detailed explanation and analysis since it has the highest R-sq (Table 3).

The MERF-XGB model identified a dozen variables to have

Table 4
Summary statistics of the GWR models in 2001, 2008, 2010, and 2018.

Year	General Info		
	Model type:		Gaussian
	Number of observations:		62
	Number of covariates:		11
	Model Summary Statistics		
2001	Log-likelihood:		−481.59
	AICc:		959.40
	R^2		0.84
	Adj. R^2		0.78
2008	Log-likelihood:		−477.97
	AICc:		961.04
	R^2		0.84
	Adj. R^2		0.78
2010	Log-likelihood:		−473.16
	AICc:		962.06
	R^2		0.85
	Adj. R^2		0.80
2018	Log-likelihood:		−482.61
	AICc:		959.41
	R^2		0.89
	Adj. R^2		0.85
	Significant Variables	T-statistic	p-value
2001	croppg	2.63	0.008
	Temp	3.12	0.002
	pcurei	2.07	0.038
	iofp	2.50	0.012
2008	croppg	4.60	0.000
	pcurei	2.08	0.037
	iofp	−2.64	0.008
	rpop	2.46	0.014
2010	Psum	−2.29	0.022
	croppg	6.86	0.000
	dustgdp	2.82	0.005
	rpop	3.48	0.001
2018	Psum	2.52	0.012
	croppg	4.13	0.000

noticeable importance affecting grassland productivity, including two climate variables (*Psum* – summarized precipitation of the growing season, and *Temp* – average temperature during the growing season), one crop plantation variable (*croppg* – the percentage of crop area and planted grassland area for harvest to the total grassland area), two industrial pollution variables (*dustgdp* – GDP per unit discharge of industrial dust, and *sdxgdp* – GDP per unit sulfur dioxide emission), and one economic indicator (*gp* – gross domestic production per capita) (Fig. 5). *Psum* had the highest mean SHAP value (0.0657). It has long been agreed that *Psum* is the most crucial driver of grassland growth in the Mongolia Plateau (Wang et al., 2013). However, this statistic only reflects an overall condition in the conventional statistics and traditional coupled human-natural system studies. In other words, the highest mean value only says that this covariate (*Psum*) has the most substantial positive influence on the target variable (the grassland productivity). Still, it fails to provide insight into how much it contributes to the model's prediction.

We conducted a panel regression-based very important feature (VIF) test using Stata 16 software to prove that multicollinearity was removed automatically. The results are reported in A-Table 7. The important features automatically selected by the MERF-XGB algorithm all passed the VIF test in a cross-section and over-time regression analysis. This finding confirmed that the machine-learning model automatically removed multicollinearity, a significant advantage for the machine-learning-based models compared to classic statistical models.

3.3. Fine-grained spatiotemporal analysis of RC variations across counties and over years

We adopted a SHAP heatmap to visualize each feature's contribution to individual prediction (EFCTIP). This facilitates researchers in understanding complex interactions between a covariate and the target variable and their case-specific variations. Fig. 6 reveals fine-grained spatial and temporal patterns of EFCTIP. The *x* axis lists the study areas (counties) by years. The *y* axis ranks each feature contribution decreasingly from the top to the bottom. They together reveal spatial and temporal variations of EFCTIC. For example, the grassland productivity curve, $f(X_i)$, was well above the average line before 2009. *Psum* was relatively abundant during this period. As a result, *Psum* exerted positive impacts on grassland productivity. However, between 2010 and 2018, the $f(X_i)$ curve was largely below the average line, and *Psum* was also under the average value. The SHAP values of *Psum* were in the blue range and became a deterring factor in grassland productivity. In other words, *Psum* did not always positively influence grassland productivity. This finding reveals our current understanding that precipitation always positively affects grassland productivity is untrue. The fine-grained analysis based on IML elucidates that the actual impact of precipitation on grassland productivity depends on its relative abundance compared with other drivers.

croppg had the second-highest mean SHAP value (0.0299), almost half of the *Psum*'s SHAP value (Fig. 5). It was also interesting to note that the SHAP values of *croppg* were almost positive (red across the entire spectrum) (Fig. 6). The *croppg* data was derived from satellite images. Crop plants and harvested grass pastures showed more greenness than natural grasslands in semi-arid and semi-humid regions (Tang, 2016). Therefore, there was a close association between croplands, harvested grass pastures, and greenness, corresponding to higher *EVI* values on the remotely sensed images.

Temp (Temperature) was the third-most important driver (Fig. 5) but showed an interesting impact pattern (Fig. 6). *Temp* displayed positive or negative impacts on grassland productivity in specific years and over certain counties. It has been controversial how *Temp* affected grassland in IMAR. Our case study confirmed that no simple linear relationship between temperature and grassland productivity could be established (Li et al., 2012). High temperatures intensified evaporation and led to drier climate conditions, negatively influencing grassland growth in semi-dried and dried regions. The drying effects of *Temp* became stronger in drought years or drier locations.

GDP per unit discharge of industrial dust (*dustgdp*) and GDP per unit sulfur dioxide emission (*sdxgdp*) were two exciting drivers of grassland productivity. They showed mixed impacts on grassland productivity (Fig. 6). For example, they had negative consequences in 2007 but positive impacts during 2010, 2011, and 2012. Moreover, the impacts of *dustgdp* and *sdxgdp* on grassland productivity displayed similar spatial and temporal variations. Although *dustgdp* and *sdxgdp* were introduced into coupled human-natural systems studies for the first time, the findings are against the common intuition that large amounts of industrial dust discharge and sulfur dioxide emission indicated fast industrialization, which led to grassland deterioration or conversion to industrial land. However, they periodically showed moderate positive influences on grassland productivity (Fig. 6, the 4th and 5th rows of *SHAP* values). We will delve into it in the next section.

Moreover, *gp (GDP* per capita) was the covariate with the sixth-highest mean SHAP value. However, the SHAP values of *gp* fluctuated frequently between red and blue, revealing that the positive or negative impacts of *gp* on grassland productivity showed apparent local variations. In some counties and years, GDP negatively affected EVI, indicating that GDP per capita would increase when a larger grassland area was converted to urban or agricultural land to seek high economic

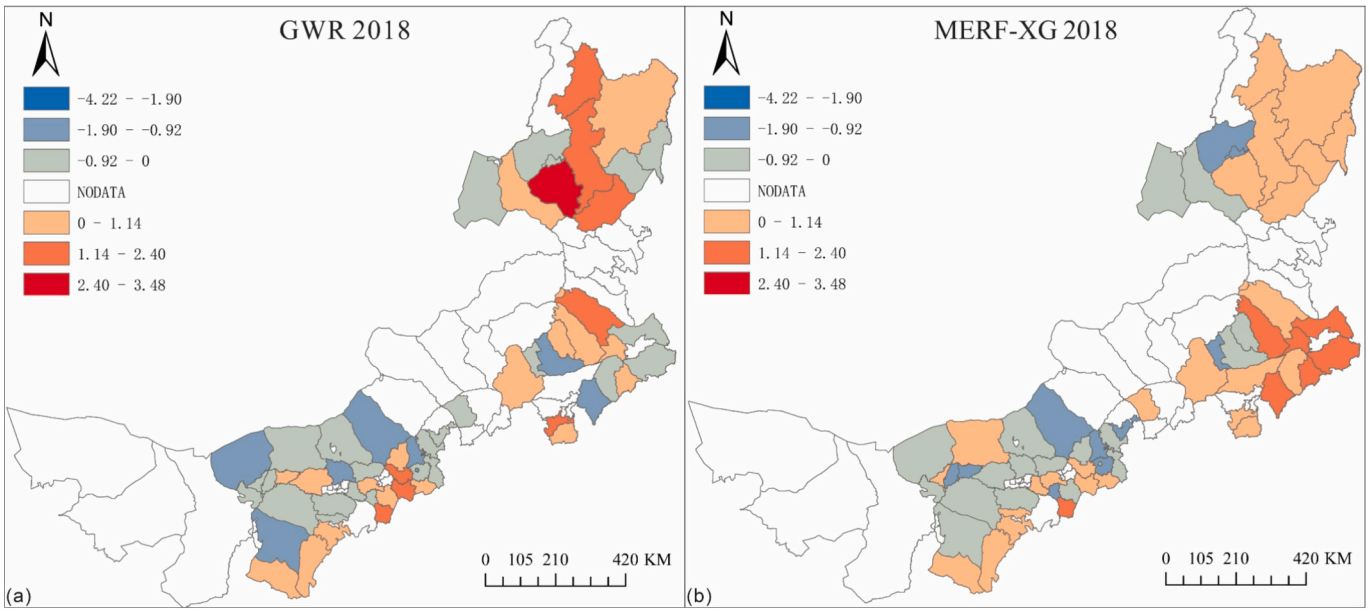

Fig. 10. (a) The spatial variations of prediction errors of the GWR model in 2018, (b) The spatial variations of prediction errors of the MERF-XGBoost model in 2018.

growth. The covariate of *gp* measures overall economic growth. The impacts of *gp* on grassland productivity varies across counties, and over time (Zhou et al., 2022).

3.4. Spatial heterogeneity of each feature's contribution to individual prediction (EFCTIP)

The x-axis in Fig. 6 lists the counties of interest by each observation year. We can zoom in for a chosen year to visualize EFCTIP in each county. Fig. 7a shows the heatmap of the important features in 2007. It is a zoomed-in heatmap of the Year 2007 in Fig. 6, which was left-turned 90 degrees. The x-axis lists the important features, and the y-axis presents the counties (banners). The map can be divided into two sections: the lower section consists of the counties and cities in the middle and west parts of IMAR, and the upper half includes the counties and cities in the east and southeast parts of IMAR. The grassland productivity curve, $f(x)$, was the primary feature that divided the study area into the eastern and the middle-western parts. This rotated heatmap is robust in revealing spatial heterogeneity of different drivers' influences on ecosystem health. For example, the middle and western parts were predominantly semi-arid and arid grasslands with relatively lower grassland productivity in 2007. The observed values of *Psum* were above the average amount in 2007, indicating a precipitation-rich year. As a result, *Psum* became the most important driving factor to *EVI* in this region (Fig. 7a). *Croppg* had a harvest year. *gp* (GDP pe capita) was higher as well. However, *Temp* differentiated its impact on *EVI* between the western and eastern sections. The western section was covered mainly by desert steppes and deserts, and *Temp* negatively affected *EVI* because it increased evaporation and air dryness. The climate in the east section was semi-humid and humid. *Temp* exhibited a positive influence. However, there were some similarities between the middle-west and the east-southeast sections. For example, *dustgdp* and *sdxgdp* displayed negative driving impacts on *EVI*. These findings suggested that IMAR was a primary animal husbandry base in 2007. Large portions of grassland and crop production helped keep animal husbandry. On the other hand, industrial development negatively impacted grassland productivity.

The year 2013 was a different year from 2007. The grassland productivity curve, $f(x)$, was under the average line in the western section and barely above the average line in the eastern section (Fig. 7b). This was a drought year. *Psum* was below the average precipitation in most counties and cities, particularly for those counties and cities located in the southern, eastern, and southeastern parts of IMAR. *Croppg* showed negative *SHAP* values across IMAR. *Temp* intensified the dryness and negatively impacted grassland productivity in many counties except those in the southeastern. In brief, animal husbandry and crop production suffered during this drought year. On the other hand, both *dustgdp* and *sdxgdp* displayed positive *SHAP* values across IMAR, contributing to *EVI*. The explanation is that industrial development-induced GDP improved the local economy. Especially when the drought negatively affected animal husbandry and agriculture production, the revenue from industrial development helped alleviate local economic stresses, reduce financial reliance on grasslands, and, thus, contribute to grassland ecosystem health.

3.5. Local analysis and visualization of EFCTIP

Spatiotemporal patterns of important features' RC provided details on how these features interacted to affect the regional pattern of grassland productivity. In addition, machine-learning techniques support examining how these important features interact with one another locally (i.e., in a particular county and at a specific year). We selected two locations (one rural banner, which is a county in the Mongolian language, and one big city) as the illustrations: Ejina Banner in 2018, and Baotou City in 2018. Ejina Banner is located far west of Inner Mongolia. Ejina has a mixed agriculture and grazing economy with a small population of 20,000∼30,000 people but has the largest grassland area among the three banners in the Alxa League. In recent years, tourism around the "Euphrates Forest, Juyanhai Lake, and Black City" flourished, which promoted the popularity of Ejina and drove the development of the tourism-related economy. Since it was located in the declining areas of *EVI* and *Pnum*, agriculture (*croppg*), grass, and their related income (*iofp*) declined. However, the industries and urban income related to tourism saw increases in 2018 (Fig. 8). The local SHAP graphic provides the observed values of all covariates on the left column and their corresponding SHAP values on the right. It illustrates the covariates' importance to local *EVI* prediction vis horizontal bars. This graphic provides fine-grained statistics and powerful visualization to reveal EFCTIP, far exceeding standard statistical approaches.

Baotou City, located in the western part of the Inner Mongolia Autonomous Region, is an important hub connecting North China and Northwest China. Baotou is one of the top three most vigorous

development areas in Inner Mongolia, along with Hohhot and Ordos. Baotou has the largest steel, aluminum, equipment manufacturing, and rare earth processing enterprises in Inner Mongolia. It is a vital energy, raw material, rare earth, new coal chemical, and equipment manufacturing base in the country and Inner Mongolia. *EVI* (grassland productivity) declined along with *Psum* since 2016. Although *EVI* started to recover in 2018, it was not back to the normal range (Fig. 6). The 2018 Baotou SHAP bar (Fig. 9) reflected this general climate change trend and Baotou industrial city characteristics. The covariates of *dustgdp* and *sdxgdp* increased, and most of the socioeconomic and new economic covariates increased. Only a few covariates such as *gp*, *pcur*ei, *Temp*, *invpa_p*, and *nosgdp* decreased.

3.6. Automatic calibration of optimal model parameters

Most machine-learning modeling frameworks support automatic calibration of optimal model parameters. We adopted Hyperopt, a Python library for hyperparameter optimization. Hyperopt's core algorithm is based on Bayesian optimization. Specifically, Hyperopt uses a Tree-structured Parzen Estimator for Bayesian optimization (Bergestra et al.). The calibrated parameters for the four machine-learning models are reported in A-Table 8. The automatic calibration of optimal model parameters is another essential improvement of machine-learning models compared with conventional statistical models.

3.7. Geographically weighted regression (GWR) models and spatial variations of ecosystem health

A GWR model was developed based on Eq. (4). The GWR model could be very complex since there exist 37 independent variables. For an illustration, the first eleven important variables identified by the MERF-XGBoost model (the top eleven variables on the left vertical axis of Fig. 6) were regressed against *EVI*. In addition, since the GWR model is not designed to handle time-series data at present, four years, 2001, 2008, 2010, and 2018, were chosen to run the GWR model. The selection of 2001 and 2018 was based on the consideration of the beginning and ending years of the study period, and also, they were the years with regular precipitation. The years of 2008 and 2010 were drought years, and 2010 was the year that witnessed dramatic socioeconomic booming, as we discussed in the study area and data section.

The key relevant parameters and statistics of the four years' GWR models are presented in Table 4, while their complete sets of outcomes are included in the Supplementary Document. The GWR model results revealed several interesting findings. First, the model's performances were judged based on linearity via the statistics, such as AICc (corrected Akaike information criterion) and adjusted R^2. Over the four years, these statistics revealed that the 2018 GWR model performed better than other years due to its normal precipitation year. Second, the significance levels of the independent variables displayed noticeable changes each year. Only two to four variables out of eleven significantly affected *EVI*, although they all were important variables contributing to *EVI* changes in the MERF-XGBoost model. Third, the climate factors, precipitation (*Psum*) and temperature (*Temp*), showed a positive influence on *EVI* in regular precipitation years but a negative impact in drought years. In summary, the interpretable machine learning based MERF-XGBoost model exhibits advantages because of its capabilities of feature engineering and non-linear relationship exploration between ecosystem health and its driving factors as discussed in the previous sections.

Next, the model prediction errors of both GWR and MERF-XGBoost models were mapped. Fig. 10a is the map of Z scores of the prediction errors by counties from the GWR model in 2018 (the maps of 2001, 2008, and 2010 are provided in the Supplementary Documents). Fig. 10b is the map of Z scores of the prediction errors by counties from the MERF-XGBoost model in 2018 (the maps of 2001, 2008, and 2010 are provided in the Supplementary Documents). The Z scores of the predicted errors can reveal the overestimation or underestimation of a regression model (Zhou et al., 2022). The positive Z scores indicated an overestimation, while the negative Z scores meant an underestimation. It was interesting to notice the differences in overestimation or underestimation between the GWR and MERF-XGBoost models.

First, two prediction error maps exhibited similar spatial patterns. The overpredictions from both models happened in the meadow grasslands in the northeastern section, the typical grasslands in the southeastern section, and the irrigated mixed agricultural lands and grasslands in the western section along the Yellow River. The underpredictions occurred in the northwestern desert grasslands. Second, the local patterns of prediction errors varied noticeably between the two models. The GWR model made overprediction errors in the central part of the northeastern section and showed varied prediction errors in the adjacent counties (Fig. 10a). However, the MERF-XGBoost model illustrated more uniform overprediction errors in this region (Fig. 10b). In the southeastern section, the MERF-XGBoost model significantly overpredicted EVI in six counties in comparison to the GWR model. In general, both GWR and MERF-XGBoost models were effective in revealing local variations.

4. Conclusions

This paper presents the first comprehensive investigation into the relative contributions of various driving factors to ecosystem health, using Inner Mongolian grasslands as a case study. The paper takes a nonlinear approach by integrating ML gradient boosting techniques with traditional cross-space and over-time panel data statistical analysis as a space–time interpretable ML application. The innovation lies in interpretability, as this paper purposefully selects ML algorithms that can explicitly examine cross-section and time series (panel) data concurrently, a desired capability that ecologists and environmental scientists are familiar with and know how to interpret.

Moreover, the ML's new capabilities, such as feature engineering and fine-grained analysis (each feature's contribution to individual forecasting), break through the limitations of classic regression-based statistical models, including linearity, multicollinearity, and system-wide interpretation. As a result, several findings from this case study have direct policy and management implications: (1) There are differentiated relative contributions (RC) of climate change, LULC, and socioeconomic factors to ecosystem health; (2) None of driving factors was predominant and showed constantly positive or negative impact on grassland health and system-wide interpretations derived from traditional models like EPRA and HLMM were misleading; (3) Strengths and directions of ecosystem sustainability driving factors' RC on ecosystem health must be understood from regional perspectives and local contexts; (4) Human-induced changes are far more important than climate change because socioeconomic and environmental factors are many; and (5) The RC differentiation has critical policy and management implications, and local governments and residents must take action to protect the grasslands because their economic activities and consumption behaviors have more profound and direct impacts on ecosystem health and recovery than climate changes.

In this paper, the enhanced vegetation index (EVI) is used as a proxy for grassland productivity to quantify ecosystem health. EVI is a crude indicator of ecosystem productivity, which is a limitation of the current dataset. More data items or variables shall be examined to represent ecosystem health or sustainability.

The inconsistent scale between datasets is another big challenge to coupled human and natural systems. In general, environmental and ecosystem data are derived from remote sensing in the format of pixels, which can be a few inches in scale. However, most current socioeconomic statistics are collected by census bureaus over counties, which cover hundreds or thousands of square kilometers. Assimilating pixel data over county boundaries loses spatial variabilities, and any analysis based on coarse county scale can lead to an oversimplified conclusion (Xie, 2023). The next experiment, extending ML functions in statistical

empirical studies, shall be conducted over fine geographical scales.

CRediT authorship contribution statement

Xiaoliang Meng: Writing – original draft, Supervision, Project administration, Investigation, Funding acquisition, Conceptualization. **Junyi Wu:** Writing – original draft, Visualization, Software, Methodology, Formal analysis, Data curation. **Yichun Xie:** Writing – review & editing, Writing – original draft, Methodology, Formal analysis, Conceptualization. **Yongfei Bai:** Writing – review & editing, Validation, Resources, Methodology, Formal analysis, Conceptualization. **Chenghu Zhou:** Writing – review & editing, Validation, Methodology, Formal analysis, Conceptualization. **Yuchen Li:** Visualization, Validation, Investigation, Formal analysis, Data curation.

Declaration of competing interest

The authors declare the following financial interests/personal relationships which may be considered as potential competing interests: Xiaoliang Meng reports financial support was provided by The Natural Science Foundation of China. If there are other authors, they declare that they have no known competing financial interests or personal relationships that could have appeared to influence the work reported in this paper.

Acknowledgments

This research has been partially funded by the National Natural Science Foundation of China (grant number 41971352).

Appendix A. Supplementary data

Supplementary data to this article can be found online at https://doi.org/10.1016/j.ecolind.2025.114087.

Data availability

The data and accompanying Python codes are freely accessible online at https://github.com/emuyxie/Differentiates-ecosystem-driving-factors-relative-contributions.

References

Andermann, T., Strömberg, C.A., Antonelli, A., Silvestro, D., 2022. The origin and evolution of open habitats in North America inferred by Bayesian deep learning models. Nat. Commun. 13, 4833.
Baltagi, B.H., 2004. 04.1.1. A Hausman test based on the difference between fixed effects two-stage least squares and error components two-stage least squares. Econ. Theory 20.
Bergen, K.J., Johnson, P.A., de Hoop, M.V., Beroza, G.C., 2019. Machine learning for data-driven discovery in solid Earth geoscience. Science 363, eaau0323.
Bergstra, J., Yamins, D. & Cox, D. D. Making a Science of Model Search: Hyperparameter Optimization in Hundreds of Dimensions for Vision Architectures.
Bolker, B. M. Linear and generalized linear mixed models. in *Ecological Statistics* (eds. Fox, G. A., Negrete-Yankelevich, S. & Sosa, V. J.) 309–333 (Oxford University PressOxford, 2015). doi:10.1093/acprof:oso/9780199672547.003.0014.
Boukari, A., et al., 2019. Assessment of agriculture pressures impact on the Joumine river water quality using the Pegase model. Environ. Manag. 64, 520–535.
Bruce, P.C., Bruce, A., 2017. Practical Statistics for Data Scientists: 50 Essential Concepts. O'Reilly, Beijing Boston Farnham Sebastopol Tokyo.
Brun, P., et al., 2024. Multispecies deep learning using citizen science data produces more informative plant community models. Nat. Commun. 15, 4421.
Celbiş, M.G., Wong, P., Kourtit, K., Nijkamp, P., 2023. Impacts of the COVID-19 outbreak on older-age cohorts in European Labor Markets: A machine learning exploration of vulnerable groups. Reg. Sci. Policy Pract. 15, 559–585.
Central Government Gate. Attach great importance to the major trend changes in China's economy. https://www.gov.cn/zhengce/2015-07/03/content_2889251.htm (2015).
Chen, M., et al., 2024. Collaboration between artificial intelligence and Earth science communities for mutual benefit. Nat. Geosci. 17, 949–952.
Chen, T., Guestrin, C. XGBoost: A Scalable Tree Boosting System. in Proceedings of the 22nd ACM SIGKDD International Conference on Knowledge Discovery and Data Mining 785–794 (ACM, San Francisco California USA, 2016). doi:10.1145/2939672.2939785.
China Meteorological Administration. 2013 CHINA CLIMATE BULLETIN. https://www.cma.gov.cn/zfxxgk/gknr/qxbg/202112/t20211228_4332030.html (2014).
Eyring, V., Gentine, P., Camps-Valls, G., Lawrence, D.M., Reichstein, M., 2024. AI-empowered next-generation multiscale climate modelling for mitigation and adaptation. Nat. Geosci. 1–9.
Fischer, J., Riechers, M., Loos, J., Martin-Lopez, B., Temperton, V.M., 2021. Making the UN decade on ecosystem restoration a social-ecological endeavour. Trends Ecol. Evol. 36, 20–28.
Forgeard, M.J., Jayawickreme, E., Kern, M.L., Seligman, M.E., 2011. Doing the right thing: Measuring wellbeing for public policy. Int. J. Wellbeing 1.
Fu, F., Jiang, J., Shao, Y., Cui, B., 2019. An experimental evaluation of large scale GBDT systems. Proc. VLDB Endow. 12, 1357–1370.
Gao, J., Li, S., 2011. Detecting spatially non-stationary and scale-dependent relationships between urban landscape fragmentation and related factors using Geographically Weighted Regression. Appl. Geogr. 31, 292–302.
Gong, P., Li, X., Zhang, W., 2019. 40-Year (1978–2017) human settlement changes in China reflected by impervious surfaces from satellite remote sensing. Sci. Bull. 64, 756–763.
Gong, E., Zhang, J., Wang, Z., Wang, J., 2024. Estimating the dynamics and driving factors of gross primary productivity over the Chinese Loess Plateau by the modified vegetation photosynthesis model. Ecol. Inform. 83, 102838.
Gupta, A.K., et al., 2020. Mapping socio-environmental vulnerability to climate change in different altitude zones in the Indian Himalayas. Ecol. Ind. 109, 105787.
Hazeleger, W., et al., 2024. Digital twins of the Earth with and for humans. Commun. Earth Environ. 5, 463.
He, L., Zhang, J., Yu, B., Hu, M., Zhang, Z., 2024. Assessment of ecosystem health and driving forces in response to landscape pattern dynamics: The Shibing Karst world natural heritage site case study. Herit. Sci. 12, 182.
Hedeker, D., Gibbons, R.D., 2006. Longitudinal Data Analysis. John Wiley & Sons.
Hsiao, C., 2007. Panel data analysis—Advantages and challenges. TEST 16, 1–22.
Hsiao, C., 2022. Analysis of Panel Data. Cambridge University Press.
Hu, Z., Dakos, V., Rietkerk, M., 2022. Using functional indicators to detect state changes in terrestrial ecosystems. Trends Ecol. Evol. 37, 1036–1045.
Huang, W., Shi, Y., Xiong, Z., Zhu, X.X., 2024. Decouple and weight semi-supervised semantic segmentation of remote sensing images. ISPRS J. Photogramm. Remote Sens. 212, 13–26.
Hull, V., Tuanmu, M.-N., Liu, J., 2015. Synthesis of human-nature feedbacks. Ecol. Soc. 20.
IMAR Statistical Bureau. Inner Mongolia Statistical Yearbook. 2000–2017.
Information Office of the Ministry of Agriculture. 2011 Outline of Policy Promotion for National Support on Increasing Grain Production and Farmer Income. https://www.moa.gov.cn/gk/zcfg/qnhnzc/201109/t20110928_2312690.htm (2011).
Irrgang, C., et al., 2021. Towards neural Earth system modelling by integrating artificial intelligence in Earth system science. Nat. Mach. Intell. 3, 667–674.
Jia, Z., Zhang, Z., Cheng, Y., Borjigin, S., Quan, Z., 2024. Grassland biomass spatiotemporal patterns and response to climate change in eastern Inner Mongolia based on XGBoost model estimates. Ecol. Ind. 158, 111554.
Kaack, L.H., et al., 2022. Aligning artificial intelligence with climate change mitigation. Nat. Clim. Chang. 12, 518–527.
Ke, G., et al., 2017. Lightgbm: A highly efficient gradient boosting decision tree. Adv. Neural Inf. Process. Syst. 30.
Kladny, K.-R., Milanta, M., Mraz, O., Hufkens, K., Stocker, B.D., 2024. Enhanced prediction of vegetation responses to extreme drought using deep learning and Earth observation data. Ecol. Inform. 80, 102474.
Kline, R.B., 2023. Principles and Practice of Structural Equation Modeling. Guilford Publications.
Koppa, A., Rains, D., Hulsman, P., Poyatos, R., Miralles, D.G., 2022. A deep learning-based hybrid model of global terrestrial evaporation. Nat. Commun. 13, 1912.
Levin, A., Lin, C.-F., Chu, C.-S.-J., 2002. Unit root tests in panel data: Asymptotic and finite-sample properties. J. Econom. 108, 1–24.
Li, S., et al., 2013. Spatial variability of the adaptation of grassland vegetation to climatic change in Inner Mongolia of China. Appl. Geogr. https://doi.org/10.1016/j.apgeog.2013.05.008.
Li, W., Wang, Y., Xie, S., Cheng, X., 2023. Exploring the regional differences of ecosystem health and its spatial relationships with urban forms in China. Environ. Sci. Pollut. Res. 30, 62000–62014.
Li, A., Wu, J., Huang, J., 2012. Distinguishing between human-induced and climate-driven vegetation changes: A critical application of RESTREND in inner Mongolia. Landsc. Ecol. 27, 969–982.
Li, S., Xie, Y., 2013. Investigating coupled impacts of climate change and socioeconomic transformation on desertification by using multitemporal landsat images: A case study in central Xilingol China. IEEE Geosci. Remote Sens. Lett. 10, 1244–1248.
Li, S., Xie, Y., Yang, Z., Lu, Y., Li, H., 2021. Examining winter fallow farmland from space and geography: A case study in Guizhou China. J. Spat. Sci. 66, 163–178.
Lu, Y., Yang, X., Xie, Y., 2024. Assessing ecological compensation policy effectiveness: A case study in the inner Mongolia autonomous region China. Sustainability 16, 8094.
Lv, X., et al., 2024. Rapid and extensive expansion of shrub encroachment into grassland in Xilin Gol League, China, and its driving forces. Int. J. Appl. Earth Obs. Geoinformation 132, 104009.
McCleery, R., et al., 2023. Uniting experiments and big data to advance ecology and conservation. Trends Ecol. Evol. 38, 970–979.
Meng, Q., et al., 2016. A communication-efficient parallel algorithm for decision tree. Adv. Neural Inf. Process. Syst. 29.
Morueta-Holme, N., Iversen, L., Corcoran, D., Rahbek, C., Normand, S., 2023. Unlocking ground-based imagery for habitat mapping. Trends Ecol., Evol.

China News Network. Memorabilia of China's telecom industry reform and restructuring and 3G development. https://www.chinanews.com.cn/cj/kong/news/2009/01-07/1518158.shtml (2009).
Norgaard, R.B., Kallis, G., 2011. Coevolutionary contradictions: prospects for a research programme on social and environmental change. Geogr. Ann. Ser. B Hum. Geogr. 93, 289–300.
Norusis, M. J. PASW Statistics 18 Advanced Statistical Procedures. (Prentice Hall Press, 2010).
O'Neill, D.W., Fanning, A.L., Lamb, W.F., Steinberger, J.K., 2018. A good life for all within planetary boundaries. Nat. Sustain. 1, 88–95.
Parente, L., et al., 2024. Annual 30-m maps of global grassland class and extent (2000–2022) based on spatiotemporal Machine Learning. Sci. Data 11, 1303.
Price, D.T., McKenney, D.W., Nalder, I.A., Hutchinson, M.F., Kesteven, J.L., 2000. A comparison of two statistical methods for spatial interpolation of Canadian monthly mean climate data. Agric. For. Meteorol. 101, 81–94.
Price, S.J., Muncy, B., Bonner, S.J., Drayer, A.N., Barton, C.D., 2016. Effects of mountaintop removal mining and valley filling on the occupancy and abundance of stream salamanders. J. Appl. Ecol. 53, 459–468.
Reichstein, M., et al., 2019. Deep learning and process understanding for data-driven Earth system science. Nature 566, 195–204.
Rudin, C., 2019. Stop explaining black box machine learning models for high stakes decisions and use interpretable models instead. Nat. Mach. Intell. 1, 206–215.
Rudin, C., et al., 2022. Interpretable machine learning: Fundamental principles and 10 grand challenges. Stat. Surv. 16, 1–85.
Schulz, M.-A., et al., 2020. Different scaling of linear models and deep learning in UKBiobank brain images versus machine-learning datasets. Nat. Commun. 11, 4238.
Shen, Z., et al., 2023. Ecological restoration research progress and prospects: A bibliometric analysis. Ecol. Ind. 155, 110968.
Shi, S., et al., 2021. Quantitative contributions of climate change and human activities to vegetation changes over multiple time scales on the Loess Plateau. Sci. Total Environ. 755, 142419.
Shiferaw, N., Habte, L., Waleed, M., 2025. Land use dynamics and their impact on hydrology and water quality of a river catchment: A comprehensive analysis and future scenario. Environ. Sci. Pollut. Res. 32, 4124–4136.
Shrestha, P., et al., 2024. Toward improved simulations of disruptive reservoirs in global hydrological modeling. Water Resour. Res. 60, e2023WR035433.
Sigrist, F., 2022. Latent Gaussian model boosting. IEEE Trans. Pattern Anal. Mach. Intell. 45, 1894–1905.
Sigrist, F., 2022. Gaussian process boosting. J. Mach. Learn. Res. 23, 1–46.
Stock, A., Gregr, E.J., Chan, K.M., 2023. Data leakage jeopardizes ecological applications of machine learning. Nat. Ecol. Evol. 7, 1743–1745.
Su, S., Lei, C., Li, A., Pi, J., Cai, Z., 2017. Coverage inequality and quality of volunteered geographic features in Chinese cities: Analyzing the associated local characteristics using geographically weighted regression. Appl. Geogr. 78, 78–93.
General Office of the State Council of the People's Republic of China. State Council Gazette No. 5, 2003. https://www.gov.cn/gongbao/content/2003/content_62103.htm (2003).
Tan, Y., Wang, Q., Zhang, Z., 2023. Coupling the linear mixed effects model with random forest improves hourly PM2. 5 estimation from Himawari-8 AOD over the Yangtze River Delta. Atmos. Pollut. Res. 14, 101739.
Tang, J., et al., 2016. Effects of excluding grazing on the vegetation and soils of degraded sparse-elm grassland in the Horqin Sandy Land. China. Agric. Ecosyst. Environ. 235, 340–348.
Tuia, D., et al., 2022. Perspectives in machine learning for wildlife conservation. Nat. Commun. 13, 1–15.
Wang, J., Brown, D.G., Chen, J., 2013. Drivers of the dynamics in net primary productivity across ecological zones on the Mongolian Plateau. Landsc. Ecol. 28, 725–739.
Waring, T.M., Goff, S.H., Smaldino, P.E., 2017. The coevolution of economic institutions and sustainable consumption via cultural group selection. Ecol. Econ. 131, 524–532.
Wegmann, M., Jaume-Santero, F., 2023. Artificial intelligence achieves easy-to-adapt nonlinear global temperature reconstructions using minimal local data. Commun. Earth Environ. 4, 217.
Weisz, H., Clark, E., 2011. Society–nature coevolution: Interdisciplinary concept for sustainability. Geogr. Ann. Ser. B Hum. Geogr. 93, 281–287.
Wu, Z., et al., 2023. Deep learning enables satellite-based monitoring of large populations of terrestrial mammals across heterogeneous landscape. Nat. Commun. 14, 3072.
Xie, Y., 2023. Total Socioenvironmental Systems: An Analytical Framework for Human-Natural Interactions and Sustainability. Springer Nature.
Xie, Y., Fan, S., Zhou, C., 2021. Examining ecosystem deterioration using a total socioenvironmental system approach. Sci. Total Environ. 784, 147171.
Yang, D., et al., 2024. Dynamic monitoring of aboveground biomass in inner Mongolia grasslands over the past 23 Years using GEE and analysis of its driving forces. J. Environ. Manage. 354, 120415.
Yang, J., Zhou, A., Han, L., Li, Y., Xie, Y., 2021. Monitoring urban black-odorous water by using hyperspectral data and machine learning. Environ. Pollut. 269, 116166.
Yuan, W., et al., 2023. A climate-water quality assessment framework for quantifying the contributions of climate change and human activities to water quality variations. J. Environ. Manage. 333, 117441.
Zhang, Y., et al., 2022. Characterization of soil salinization and its driving factors in a typical irrigation area of Northwest China. Sci. Total Environ. 837, 155808.
Zhou, C., Xie, Y., Zhang, A., Liu, C., Yang, J., 2022. Spatiotemporal analysis of interactions between seasonal water, climate, land use, policy, and socioeconomic changes: Hulun-Buir Steppe as a Case Study. Water Res. 209, 117937.